

Characterisation and monitoring of oil-well cements under simulated CCS well conditions

CEMENTTEGRITY Deliverables 5.1 – 5.6, v. 1
Published 2025-03-31

Authors: Benny Suryanto, Gerard Starrs
Heriot-Watt University, Edinburgh, United Kingdom

Keywords: *cement plug, bond integrity, interface condition, impedance spectroscopy, resistance.*

Summary:

This document provides a summary of the work undertaken as part of Work Package 5 at Heriot-Watt University.

1. Introduction

In light of the projected timescales envisaged for the operation of CCS storage facilities, which is well in excess of the lifespan of traditional oil and gas wells, minimising the leakage of CO₂ is of utmost importance for effective CCS storage performance. **Figure 1** shows a schematic representation of the structure of a plugged wellbore, illustrating the natural rock formation and the steel casing of the well-head, with the potential pathways for leakage of CO₂ highlighted. These pathways include leakage through the external casing/well-head interface, the internal casing/well-head interface, the well-head microstructure and/or internal fractures, as well as the external cement sheath/rock interface.

To minimise the risk of CO₂ leakage, whether in its liquid, dissolved, or gaseous form, it is essential to ensure good adhesion between the well-plug, the surrounding rock formation, and the wellbore casing. Historically, the adhesion of well-plug sealant materials to the surrounding casing or rock formation has been assessed using a variety of bond tests (e.g., shear bond test, hydraulic bond test, gas bond test, or a combination thereof). Shear bond measures the shear strength of an interface and is generally obtained by measuring the force required to initiate movement of a cement plug encased in a metal cylinder, or a pipe or rod embedded in a cement cylinder. Hydraulic bond evaluates the resistance between cement and surrounding casing and/or formation to fluid migration and is typically assessed by measurement of the flow of hydraulic fluid through an interface over time. The principle of gas bond is similar in many respects to hydraulic bond but relies on the measurement of gas migration instead of fluid migration. Due to the nature of the tests, hydraulic and gas bond can be expected offer a more direct representation of interface leakage performance. However, the tests are generally much more difficult to perform and more sensitive to experimental errors caused by gas leakage from the pressure containment cell and ballooning effects.

Within the CEMENTTEGRITY project (www.cementgrity.eu), Heriot-Watt University is responsible for delivering Work Package (WP) 5, which centres on the characterisation of the interfacial and bulk properties of cement sealants. To this end, we have developed laboratory-based test procedures designed to assess the shear bond strength of cementitious sealants encased within rigid (in this case, metal) cylinders. The following sections detail the test methodology, focusing on test procedures that can be easily implemented within standard cement and concrete testing laboratory facilities. This report also outlines how this test methodology is applied to evaluate the bond performance of CEMENTTEGRITY sealants. The majority of the test samples were subjected to an enhanced curing regime, intended to achieve thorough hydration within the timeframe of the project and replicate certain aspects of the high-

temperature and high-pressure conditions typical of a subsea wellbore. Non-destructive testing methods, employing electrical property measurements, were also conducted in parallel with the shear-bond tests, both during and after the enhanced curing process, to provide insights into the bulk properties of the sealants and additional information for future classification and performance evaluation. The findings from this WP complement the results obtained using various investigative techniques across other WPs in the CEMENTTEGRITY project. This report provides a summary of the scope, methodology, and key outcomes of WP 5.

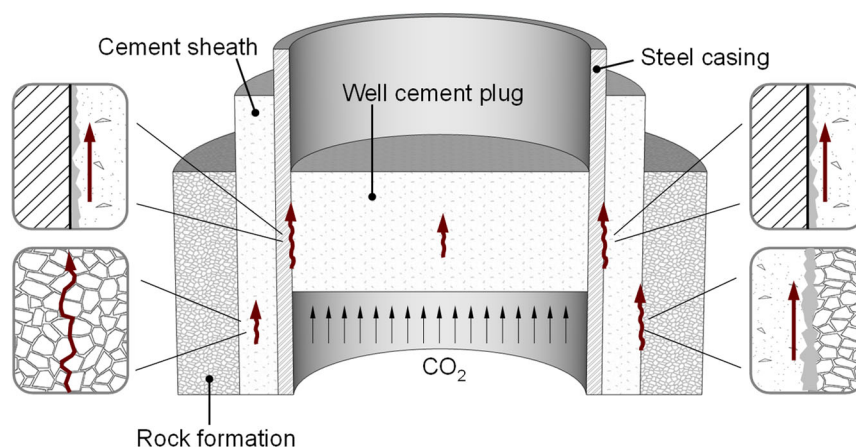


Figure 1. Schematic representation of possible leakage pathways in a CCS well.

2. Experimental Programme

2.1 Materials

The sealants used in this WP are presented in **Table 1**, together with their respective specific gravity and technology readiness level (TRL). Sealant S1 is a representative of material used for old oil and gas wells and contains a standard Portland cement Class G and silica flour (35% by weight). The other sealants are proprietary materials whose details cannot be fully disclosed. Sealant S2 is also a representative of a wellbore plugging material, containing an expansive agent and mineral addition, designed particularly to produce very low permeability. Sealant S3 is a modified version of Sealant S2 and contains additional CO₂ sequestering mineral additives, namely RePlug®. S4 is a proprietary calcium aluminate system currently deployed in high temperature wells and considered highly acid resistant. Sealant S5 is a geopolymer sealant utilising a mixture of precursors and include granite as filling materials. Sealants S3, S4, and S5 are all designated proprietary blends for new CCS wells. A typical oxide composition of the Portland cement is presented in **Table 2**.

Table 1. Summary of sealant materials.

ID	Description	SG	TRL
S1	Standard Portland cement (PC)-silica blend	1.9	7
S2	Reduced permeability PC-silica blend for field use	1.9	7
S3	PC-silica blend with reduced permeability, containing CO ₂ sequestering mineral additive RePlug®	1.9	3
S4	Calcium aluminate cement-based blend	1.8	7
S5	Geopolymer using granite as one of the precursors	1.9	3

Table 2. Oxide analysis of Portland cement.

CaO	SiO ₂	Al ₂ O ₃	Fe ₂ O ₃	MgO	MnO	TiO ₂	P ₂ O ₅	Sr	SO ₃	K ₂ O	Na ₂ O
62.0	19.63	4.08	5.94	1.19	0.12	0.25	0.08	0.17	4.08	0.81	0.17

The test sample for the bond test took the form of miniature versions of a plugged wellbore, comprising outer cylindrical steel casing and internal cement plug, see **Figure 2**. The steel casing had an outside diameter of 50.8 mm and a wall thickness of 3.2 mm. The choice of the steel casing diameter was determined by the internal diameter of the autoclave used for the enhanced curing, ensuring it could accommodate five samples per height (arranged in a star-like pattern), with four positioned around the edges and one placed centrally in the middle. The use of mild steel casing (Grade CFS 3BK) instead of super duplex steel (used typically for CCS well) was sought by the project consortium at the onset of the project to allow for possible occurrence of corrosion to take place, in addition facilitating the machining of the two ends of the tube.

At the outset of the project, three varying lengths of steel casing (25 mm, 50 mm, and 70 mm) and diameters (30.8 mm and 50.8 mm) were examined to assess their influence on bond strength, failure mode (either shear sliding or sealant crushing), and the maximum load relative to the capacity of the test machine. These tests were undertaken under controlled laboratory conditions of 20°C and ambient pressure, with test specimens cured for 90 days. Based on these preliminary tests, the 50 mm length was selected, as depicted in the schematic in **Figure 2**. This choice provides a balance by minimising fabrication errors associated with shorter specimens (25 mm), while ensuring that failure is due to shear sliding rather than crushing. Additionally, the maximum loads applied were within the load capacity of the test machine, ranging from 9.0 kN for 25 mm samples to 16.1 kN for 50 mm samples, and further increasing to 28.8 kN for 70 mm samples. This allowed ample margin for testing the primary test samples. As the main samples were later cured under the enhanced regime (detailed below) and were expected to exhibit significantly greater strength, the decision was made to proceed with the 50 mm option.

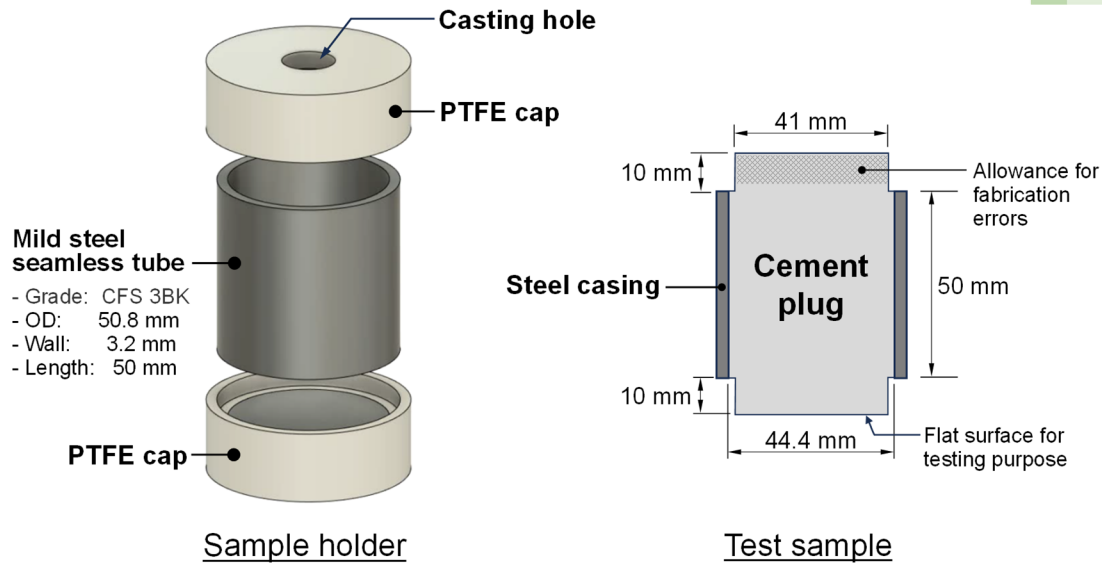


Figure 2. Schematic of test sample representing a miniature of a plugged wellbore.

The internal sealant cement plug had a diameter of ~44.4 mm and a 10 mm protruding end on either side, which had a diameter of 41 mm. These protruding ends were provided to minimise the boundary effects during mechanical bond testing: the top part was provided to remove the undesirable effects from the presence of relatively poor quality of material and uneven surface at the top during sample preparation, whereas the bottom part was to minimise stress concentration during testing. The manufacture of this protruding shape was facilitated by two PTFE end caps which encapsulated the sealant during sample fabrication and curing. The top PTFE cap had a 20 mm central hole for casting purposes, while the bottom cap was fitted without any alteration to provide a flat surface for bond testing.

Samples designed for electrical measurements were equipped with embedded electrodes to facilitate data collection. During the initial trials, a vertical arrangement of stainless-steel rings positioned along the centreline of the samples was utilised. It was observed that this electrode configuration imposed excessive restraint on the sealant during high-temperature curing, resulting in the formation of significant radial cracking in the sealant material, which rendered the samples produced during the first batch for further testing. Consequently, the electrode design was modified to mitigate these issues.

The final electrode design employed two miniature electrode configurations: the 2-pin parallel pair and the 1-pin coaxial, see **Figure 3**. The electrodes were significantly smaller relative to sample size to minimise restraint, thereby reducing the likelihood of cracking during high temperature curing. In the 2-pin parallel-

pair configuration, two marine grade steel rods, each 2.4 mm in diameter and spaced 15 mm (centre-to-centre), were positioned along the full length of the sample, to obtain its bulk electrical properties. Conversely, the 1-pin coaxial configuration utilised a single 2.4 mm diameter rod positioned along the centreline of the sample as the first electrode, with the steel casing serving as the second electrode. This coaxial configuration enabled impedance measurements through the sealant material and at the sealant/casing interface, thereby facilitating the assessment of the interface.

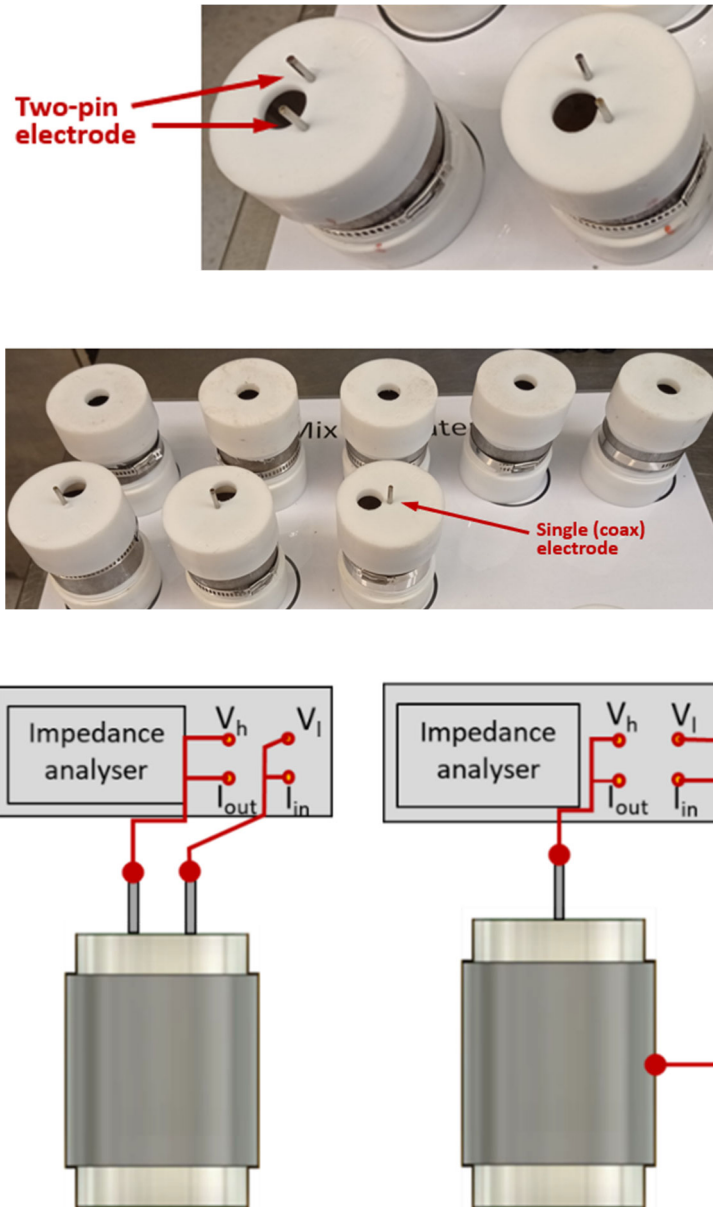


Figure 3. Schematic of 2-Pin (left) and Coaxial (right) electrode configurations.

2.2 Sample fabrication and curing

Prior to the fabrication of the main test samples, each steel tube was cut to length (i.e., 50 mm) and then immersed in a water-based degreasing solution for 24 hours. The inner and outer faces of the tube were then thoroughly wiped with paper towels. This process was repeated one time to ensure that any oils that were present on the inner face of the tubes (required for cutting and milling) were fully removed. After thoroughly cleaned, the steel tubes were then transported to Norway for sample fabrication purpose. For each sealant material, a total of 14 samples were prepared: six designated for bond testing to evaluate the shear bond strength, another six allocated for electrical testing to measure impedance properties and conductivity, and the remaining two retained as spare samples. All mixes were prepared by the technical team at Halliburton in Norway, in accordance with API Recommended Practice 10B-2, with the casting done immediately after by the HWU staff. Sealants S1 and S2 were manufactured on the same day, and the same with Sealants S3 and S4. Sealants S5 were manufactured with sealants S4 (repeat) and S1 (repeat). The fabrication of all sealants followed the same sample preparation procedure to allow for direct comparisons. Additional samples of Sealant S1 were fabricated in the UK, as this was the only non-proprietary sealant mix available for the study. This enabled further investigation into the factors thought to influence the test results, providing a more comprehensive understanding of the variables affecting the sealant performance under the simulated wellbore conditions.

With regards to curing, as illustrated in **Figure 4**, an autoclave was employed to subject the test samples to elevated temperature and pressure shortly after fabrication, within 30-45 minutes of gauging with water. Two different curing media were used: water for the majority of the samples and oil for two samples with the 2-electrode configuration, to allow for the monitoring of the bulk electrical response during the curing process. The autoclave system was pressurised to 300 bars (equivalent to ~3000 m below sea level), then the internal temperature was raised over a period of 4 hours from 20°C to 80°C where it was held for 3 days. This 80°C temperature was selected based on the minimum CCS operational temperature and practicality during bond testing. The temperature was then raised from 80°C to 150°C over 7 days and held at 150°C for a further 21 days. At this point (31.33 days after pressurisation), the temperature was reduced steadily from 150°C to 20°C over a period of 7 days. When 100°C was reached during this phase, the internal pressure was released to allow the chamber to reach equilibrium (in terms of pressure and temperature).

During the high temperature curing, Resistance data was gathered every 30 minutes to track the sealant hydration and hardening process. At the end of the curing regime, all samples were placed in water under wet hessian cloth in sealed plastic containers and air transported from Norway to HWU in the UK. The sample containers were then stored at laboratory temperature ($20\pm 1^{\circ}\text{C}$) until required for testing.

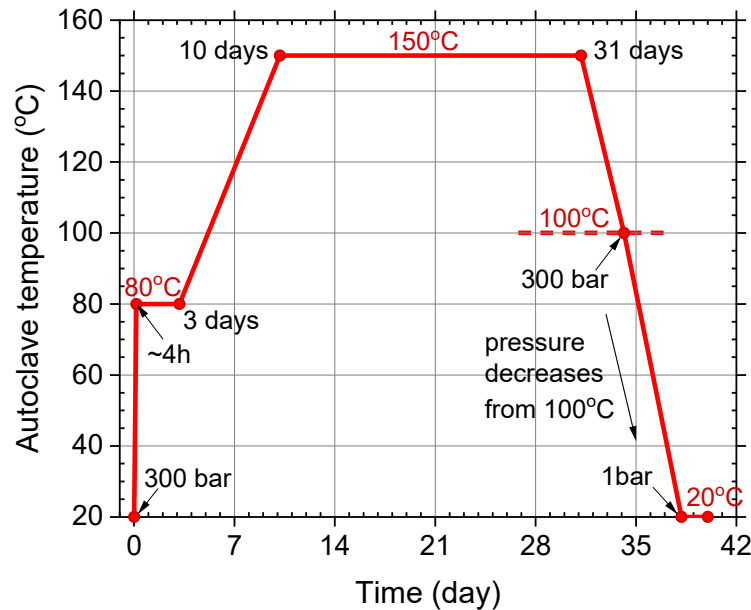


Figure 4. Schematic representation of the curing regime.

2.3 Electrical measurements during curing

Once the slurry was sealed in the casings, the samples were placed in the autoclave chambers in an aqueous containment fluid. For each sealant type, two samples of the 2-pin electrode type were connected to a logging system capable of tracking *in-situ* low frequency (i.e. direct electrical current) Resistance during the curing period. As noted above, these samples were housed in a separate chamber with an electrically inert mineral oil containment fluid to prevent contamination of the electrical measurements. A bespoke logging system was used, comprising a programmable logger that generates a square wave measurement voltage of 1 V peak-to-peak and stores the current response of each sample as a resultant Resistance value. The logger was interfaced to the samples via a multiplexer unit that allows up to 72 separate measurements per cycle. The logger and multiplexer units, along with the autoclave system and 2-pin electrode samples ready for containment in the autoclave system, are shown in **Figure 5**. Each sample was connected to thin lead wires that were interfaced to the multiplexer via a special 8-wire feedthrough connector.

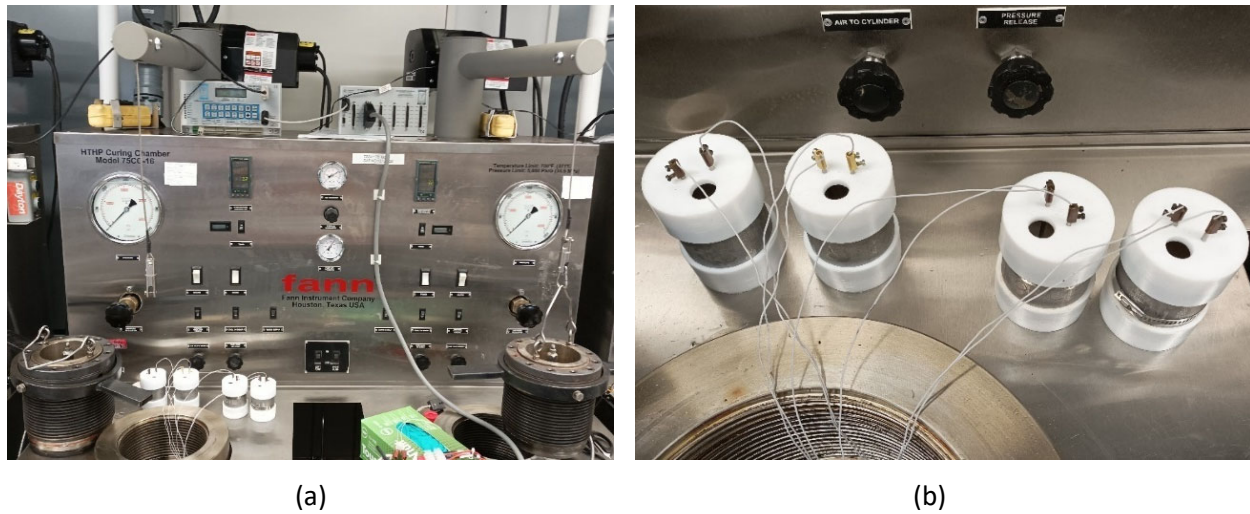


Figure 5. (a) Logging system placed above the two-chamber autoclave and (b) 2-pin electrode samples ready for testing.

2.4 Shear bond testing

One day prior to bond testing, all samples were pre-conditioned in an environmental chamber to increase the sample temperature back to 80°C over a period of 24 hours. During this pre-conditioning stage, all samples were kept in water to buffer the temperature. Bond testing was then performed using a 100kN Instron 5892 testing machine. The experimental setup, illustrated schematically in **Figure 6**, adhered to the test procedures essentially outlined in Patent No. NO20191422 (US11054353B2), with some adjustments applied earlier to facilitate the curing of test samples under elevated temperature and pressure detailed above while preventing the formation of cracks that would compromise the samples for further testing.

Prior to the commencement of each test, each sample was removed from the chamber and then tightly wrapped with a 30 mm-thick pipe insulation to minimise temperature loss. The sample was then placed on a central-hollow steel bracket (pre-conditioned at 80°C) in an upside-down position to present the flat face of the sample to the loading plate on top. The load was then applied through a hemispherical steel plate placed on the top of the sealant in a force-controlled manner, at a rate of 5 kN/min. The machine automatically stopped when a sudden drop of resistance (i.e., > 20%) occurred, due to either sliding or crushing of the inner cement plug. Each test took approximately 5 to 10 minutes to complete and hence can be considered as being quasi static in nature.

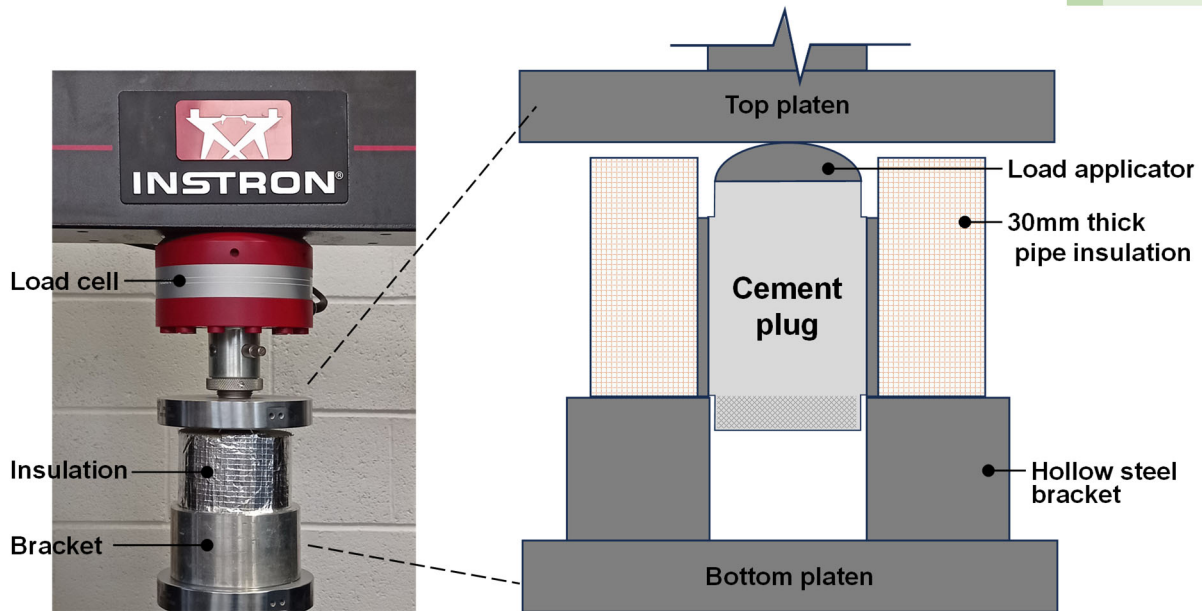


Figure 6. Schematic diagram of bond test.

The apparent mean bond stress, τ (MPa), during testing can be calculated as

$$\tau = \frac{P}{A} \quad \text{Eq. (1)}$$

where P is the applied load (in N) and A is the contact area between the sealant and steel casing (approximately $44.4 \times 50 \text{ mm}^2$).

2.5 Exposure test: accelerated corrosion

The formation of corrosion products within confined spaces, such as the sealant/casing interface, can lead to the development of internal confining stress due to the expansive nature of corrosion. This can, in turn, enhance bond strength. To investigate the influence of confining stress on bond strength, two series of additional tests were undertaken.

In the first series, test samples were fabricated under standard laboratory conditions, at a temperature of 20°C and normal atmospheric pressure. The second series involved fabricating test samples under enhanced temperature and pressure conditions, as previously applied. Accelerated corrosion tests were carried out on the samples to evaluate their corrosion potential and bond strengths after exposure. The purpose of the initial series was to identify suitable current levels and replicate the conditions of sealant S1 following enhanced (autoclaved) curing, during which significant corrosion was observed. These tests

were conducted on the S1 sealant, referred to as LabCorr samples. The second series of tests included all sealants and is referred to as CemCorr samples.

A schematic diagram of the accelerated corrosion tests and the corresponding samples is presented in **Figure 7**. Each sample contained 2.4mm diameter stainless-steel rod embedded along the longitudinal axis of the sample at the time of casting. These samples were stored under water for 25 days. As illustrated in the schematic diagram, the lower part of the samples was immersed in water in a small plastic container. On the same day (Day 26), four of the samples were connected to a DC power supply to artificially induce corrosion. This was done by connecting the stainless-steel central rod to the positive terminal of the power supply (acting as a cathode) and the metal casing to the negative terminal (acting as an anode). Two of the samples were exposed to a constant current of 15mA and the other two to 30mA, corresponding to an average current density of 0.21 and 0.42 mA/cm², respectively. They were connected to the power supply for 6 days, followed by 1 day rest to allow for various measurements to be undertaken (discussed in another article). This continued on a weekly basis until required for bond testing at 90 days. The remaining three samples were left unconnected and used as a benchmark. During the testing period, half-cell potential measurements were taken (between the stainless-steel rod and the mild-steel casing) to evaluate the likelihood and presence of corrosion.

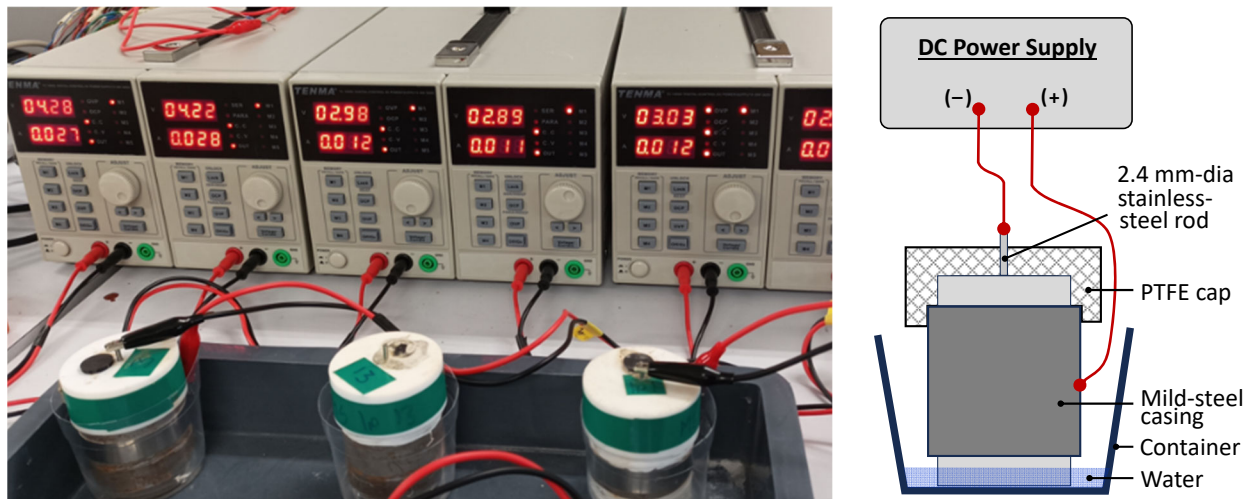


Figure 7. Photo and schematic diagram of accelerated corrosion exposure test.

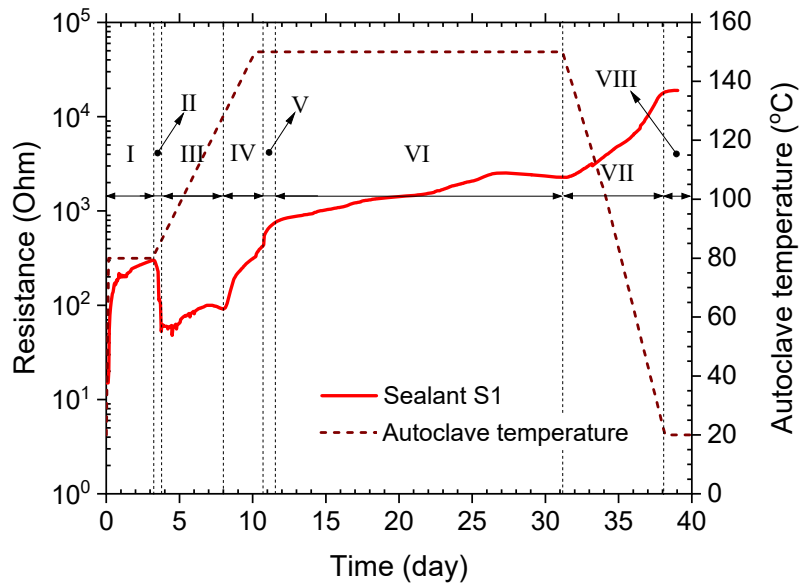
3. Results and Discussion

3.1 Electrical measurements during enhanced curing

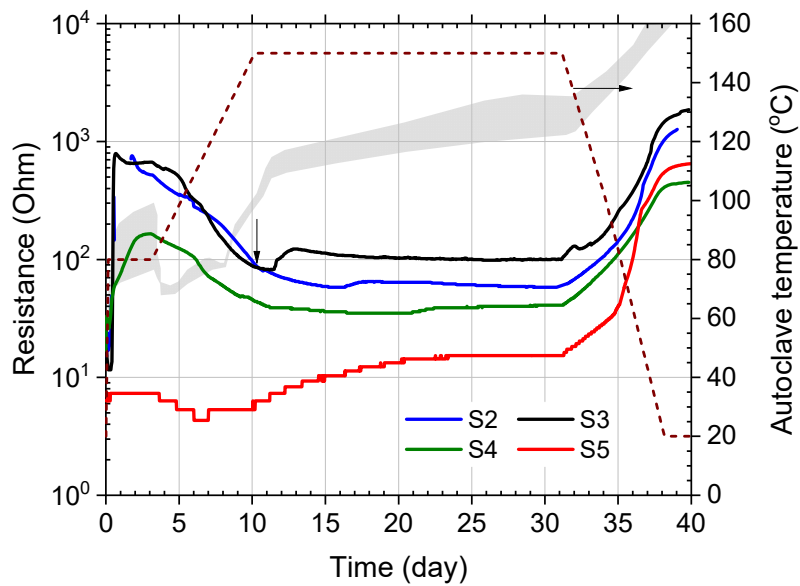
The Resistance of the sealants can be expected to be thermally activated, displaying a negative temperature response with Resistance (i.e., decreasing as temperature increases). However, because the microstructural characteristics (hence availability of conduction paths) as well as the ionic content (hence conductivity) of the pore solution are in a state of change (particularly in the early stages of curing, both pre- and post- setting), the Resistance of the sealants Resistance is a result of competing effects.

Figures 8(a) and (b) illustrate the Resistance profiles of all sealants during the enhanced curing process presented along with the temperature profile. Referring to the response of Sealant S1 in **Figure 8(a)**, during the initial 3 days at 80°C, a gradual increase in Resistance was observed reflecting early development of a pore structure due to Portland cement hydration (Stage I). The trend was then reversed briefly once temperature started to increase (Stage II), with Resistance dropping with increasing temperature. This resulted from the temperature effects noted above. However, in less than one day, as temperature continued to increase, the accelerating hydration and pore development overcame this trend, causing the Resistance to increase again (Stage III). The rate of the Resistance increased becomes more pronounced at around 130°C (Stage IV) and 150°C (Stage V), likely indicative of the active engagement of silica flour in the hydration process. Once the temperature was stable at 150°C, the Resistance continued to increase at a lower rate, revealing continued development of the microstructure as hydration proceeded. The Resistance appeared to level off towards the end of Stage VI, indicating that the material has reached full hydration. Shortly after 31 days, the temperature was steadily reduced from 150°C to 20°C, causing the Resistance of the cured material to increase towards a much higher value following its negative temperature response before plateauing (Stage VIII).

The Resistance profiles of sealants S2, S3, S4 and S5 are shown in **Figure 8(b)**, along with the Autoclave temperature profile and variation in the Resistance of Sealant S1 (shown in shaded grey area). As with Sealant S1, the Resistance was observed to be correlated to temperature throughout curing, but with each sealant showed measurably different absolute values of resistance as well as individual distinguishing characteristics as hydration reactions proceeded. Such pattern modifications at key stages were due to the specific individual materials and additions present in the sealants. For example, Sealants S2 and S3 samples displayed similar curing profiles in the early stages, which is characterised by a rapid increase in Resistance at approximately 6 hours after the temperature had reached 80°C. While the temperature was



(a)



(b)

Figure 8. Resistance profile: (a) Sealant S1 and (b) Sealants S2–S5 during enhanced curing.

held constant at 80°C (during Stage 1), Sealant S2 sample displayed a falling Resistance (possibly as a result of dissolution), whereas the Resistance of Sealant S3 sample remains steady, likely signifying the engagement and dissolution of the ReStone[®] mineral component in the hydration process. During the temperature rise from 80°C to 150°C , both sealants displayed a steady fall in Resistance. Sealant S3 sample had a small sudden rise in Resistance at approximately 29 hours after reaching 150°C that quickly levelled off, possibly indicating further engagement of the ReStone[®] mineral component in the hydration

process. Sealant S5 sample, the one-part geopolymer, had the simplest response of the sealants. It showed no notable change in Resistance while temperature was held at 80°C during Stage I indicating the competing effects of dissolution and pore formation at this early stage. As temperature increased towards 150°C, the Resistance initially dropped as would be expected due to temperature effects. However, this response was reversed at 7 days when the temperature reached around 120°C at which point the Resistance began to increase, indicating development of a rigid material with a pore structure gradually being infilled by precipitating hydration products. The increase continued until 23 days then levelled off as curing was approaching completion. Finally, all sealants showed a similar general steep rise in Resistance as the temperature decreased from 150°C to 20°C at the end of curing due to temperature effects on conduction but the individual rate and profile for each suggests distinguishable thermal activation characteristics which will be discussed below.

3.2 Mean bond strength and stiffness

Figures 9(a)–(c) display the mean bond stress vs top displacement relationships for the initial four sealants, with each Figure comparing the results of three notionally identical samples for each sealant with those of Sealant S1. The results for Sealant S5 samples are explained in the following section, as this batch was tested during the second half of the project with a different reference. In general terms, the comparisons presented indicate that all sealant samples displayed a similar increase in the mean bond stress with increasing displacement until failure, which occurred suddenly due to sliding of the sealant in the vertical direction.

The results presented in **Figures 9(a)–(c)** show that the individual sealants exhibited varying bond strengths and overall stiffnesses, with both parameters decreasing in the order: S1 < S3 < S2 < S4. For instance, in case of Sealant S2 samples, the mean bond strength and stiffness were 1.51 MPa and 8.95 N/mm³, which are only 32.5% and 80.6% of those of Sealant S1 samples, respectively. Sealant S3 samples exhibited higher mean bond strength and stiffness, with mean values of 3.54 MPa and 9.20 N/mm³, corresponding to 75.9% and 82.9% of those of the reference value, respectively. Sealant S4 samples demonstrated the lowest mean bond strength (= 0.54 MPa), which is only 11.5% of that of the reference sealant, and the lowest overall stiffness (= 2.88 N/mm³, or only approximately 26% of that of Sealant S1). This might be attributed to sliding shear movement between the sealant and the steel casing during testing.

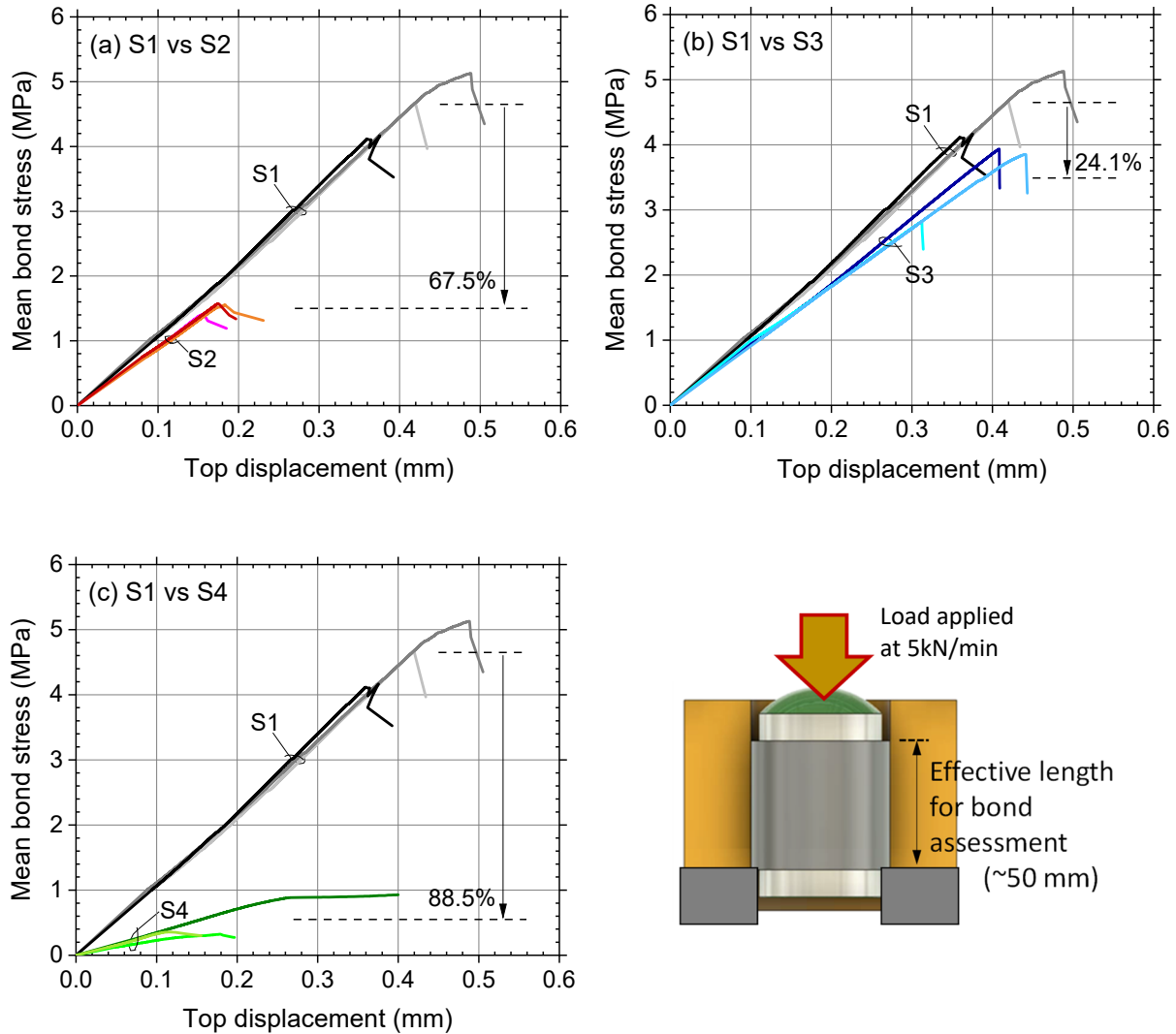


Figure 9. Mean bond stress–top displacement for Sealants S1–S4.

Direct comparisons of the mean bond strengths obtained from previous studies are difficult due to the scarcity of published values, with most samples being cured at ambient or limited curing pressure. However, some comparisons are provided in **Figure 10(a)**. It is of interest to note that the mean bond strengths of Sealants S2 and S4 samples lie within the range of reported values, whereas those of Sealants S1 and S3 samples are generally higher. Interestingly, the mean bond strength of Sealant S2 samples (= 1.51 MPa), which contains expansive agent, is comparable to the 1.5 MPa average reported recently by Kamali *et al* (2022), which was obtained from cement test samples containing magnesium oxide expansive agent. By contrast, the mean bond strength of Sealant S1 samples (= 4.66 MPa) is much higher than the 0.6 MPa average obtained from the same study, measured on Portland cement (type G) cement samples encased in metal casing; these samples were cured in 90°C chamber at 34 bars for only 7 days. **Figure 10**

also shows that the mean bond strength of Sealant S1 samples is also higher than the 1.4–3.1 MPa range obtained from metal pipe encased in sealant, and the range 0.12–0.26 MPa reported by Mabeyo *et al.* (2020) for cement samples encased in cement mortar and cured in 80°C water bath at ambient pressure over a 28-day period. Therefore, it is possible that the lower bond strength of Sealants S2 and S4 observed earlier in **Figures 9(a) and (c)** is not due to their reduced strengths, but rather because of the elevated bond strengths of Sealant S1 and S3. In addition to bond strength, the apparent stiffness determined from the shear bond test can also be analysed. The overall stiffness of the curves can be mainly attributed to the deformation of the top protruding part of each sample under loading and the initial slip between the sealant and the metal casing during bond testing, in addition to the deformation of the entire test setup, which can be expected to be similar for all samples. Therefore, comparing the overall stiffness obtained from each sealant with their modulus of elasticity (MOE) could provide an indication of the extent of initial slip experienced during the test.

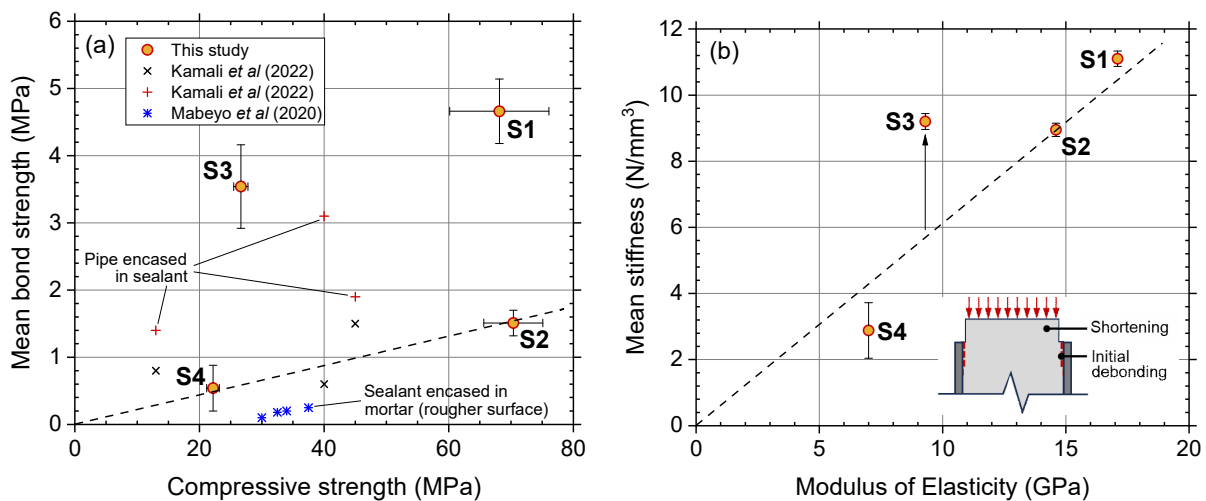


Figure 10. Comparisons of bond test results with basic mechanical properties.

Figure 10(b) compares the overall stiffness obtained from each sample plotted against their respective MOE value. Note that the MOE of each sealant was measured in WP 1 on notionally identical materials cured at 150°C and 300 bar for 28 days, producing compressive strengths of 107, 76, 32, 21 MPa for Sealants S1 to S4, respectively. It is evident from the Figure that the overall stiffness obtained from bond testing exhibits an almost linear relationship with MOE. The only exception is Sealant S3, which displayed higher stiffness than the linear relationship (indicated by an arrow). This indicates that this sealant might have experienced less sliding during bond testing than the other sealants. Sealant S4 exhibited slightly

lower stiffness than the average (represented by the trendline), suggesting the occurrence of comparatively greater initial slip during bond testing. To understand the contributing factors, the internal sealant plug was extracted from the metal casing post-testing and is discussed below.

3.3 Inner surface conditions and failure mechanisms

On completion of the bond testing, each sample was machined to extract the internal cement plug from the steel casing to allow the condition at the sealant/steel casing interface to be visually inspected. This was done by milling into the outer surface of the steel casing to create a longitudinal recess steadily until it cut through the entire thickness of the steel. Upon completion of this process, the cement sealant was extracted and then photographed. This was done by placing a sealant sample at a fixed distance from a DSLR camera and taking multiple photos while rotating the sample. Twelve images were acquired from each sample to ensure sufficient overlap between images for stitching. These images were then corrected for distortion in Adobe Photoshop and stitched together using the Photomerge feature in the software.

Figure 11 displays the acquired images from each sealant sample. Sealant S1 samples displayed a significant presence of corrosion products on the entire surface of the sealant, primarily in dark brown and black colours. Few patches of the original surface of the sealant were apparent as the rust layer came off during the extraction, or due to the milling process as shown in the right-hand side. Sealant S2 samples displayed an interesting surface pattern, comprising small white/light-grey patches dispersed across a darker grey background. On examination, the white/light-grey zones were found to be the material that had been directly adhered to the steel surface but had separated under the application of shear load. The darker background is the exposed sub-surface of the sealant material immediately beneath the sealant/steel interface, an effect resulting from the separation of the still adhering sealant surface from the sample body. Thus, it is inferred that apparent bond failure of the S2 samples results from a combination of material failure beneath the steel/material interface, and *partial* failure of the sealant/steel bond. Sealant S3 samples, like Sealant S2, displayed only a minor extent of corrosion, concentrated primarily at both ends of the sample. In contrast, however, Sealant S3 samples exhibited a clean surface representing the appearance and texture of hardened cement paste in general. As shown in **Figure 12**, the inner surface face of the tube was also relatively clean, with a minor extent of corrosion present. This would indicate that failure of Sealant S3 samples was governed by bond failure at the interface between the sealant and metal casing. Sealant S4 samples displayed a moderate level of

corrosion (brighter in colour) and the presence of a failure surface where a layer of the sealant material near the interface spalled off. Other than these regions, the remaining surface appeared to be clean.

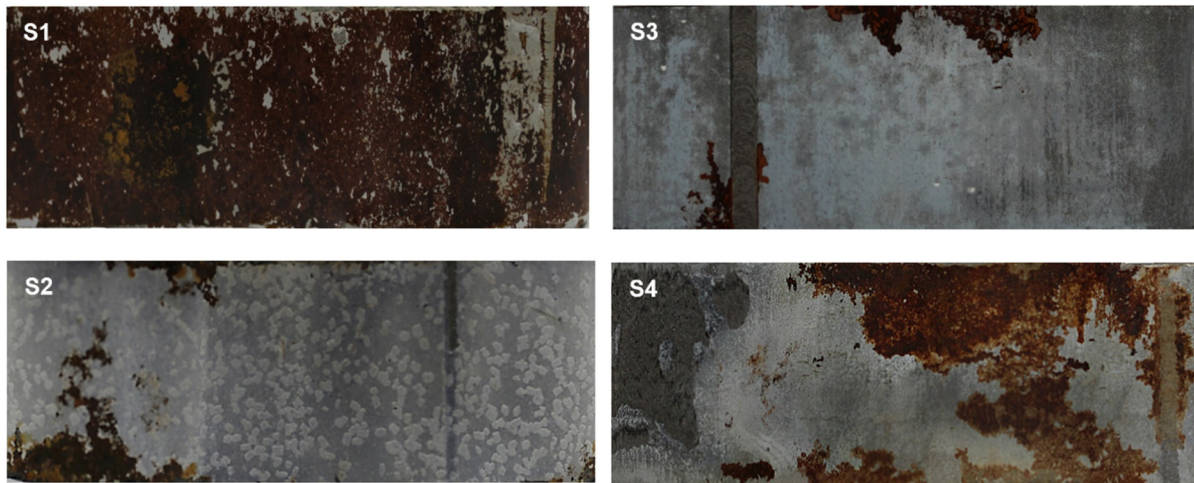


Figure 11. Montage of the sealant surface post testing.

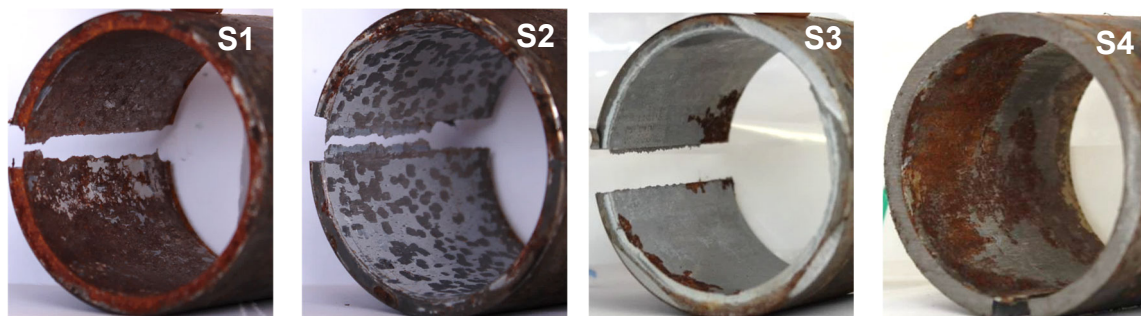


Figure 12. Surface condition of the inner pipe post bond testing.

3.4 Post exposure bond strength: effect of corrosion

Figure 13 displays the 90-day mean bond stress vs top displacement relationships for the three groups of S1 sealants, with the tests performed at 20°C and under a crosshead speed of 0.2 mm/min. It is evident that there is a noticeable difference in bond performance between the three groups of samples in terms of bond strength and overall stiffness. In general, an increase in the 90-day mean bond strength with increasing current levels is evident, from 0.91 MPa at 0 mA to 1.19 MPa at 15 mA (or 30.8% increase) and 3.18 MPa at 30 mA (349% increase). This confirms the above postulate that the enhancement in bond strength is affected by the extent of corrosion at the sealant/casing interface.

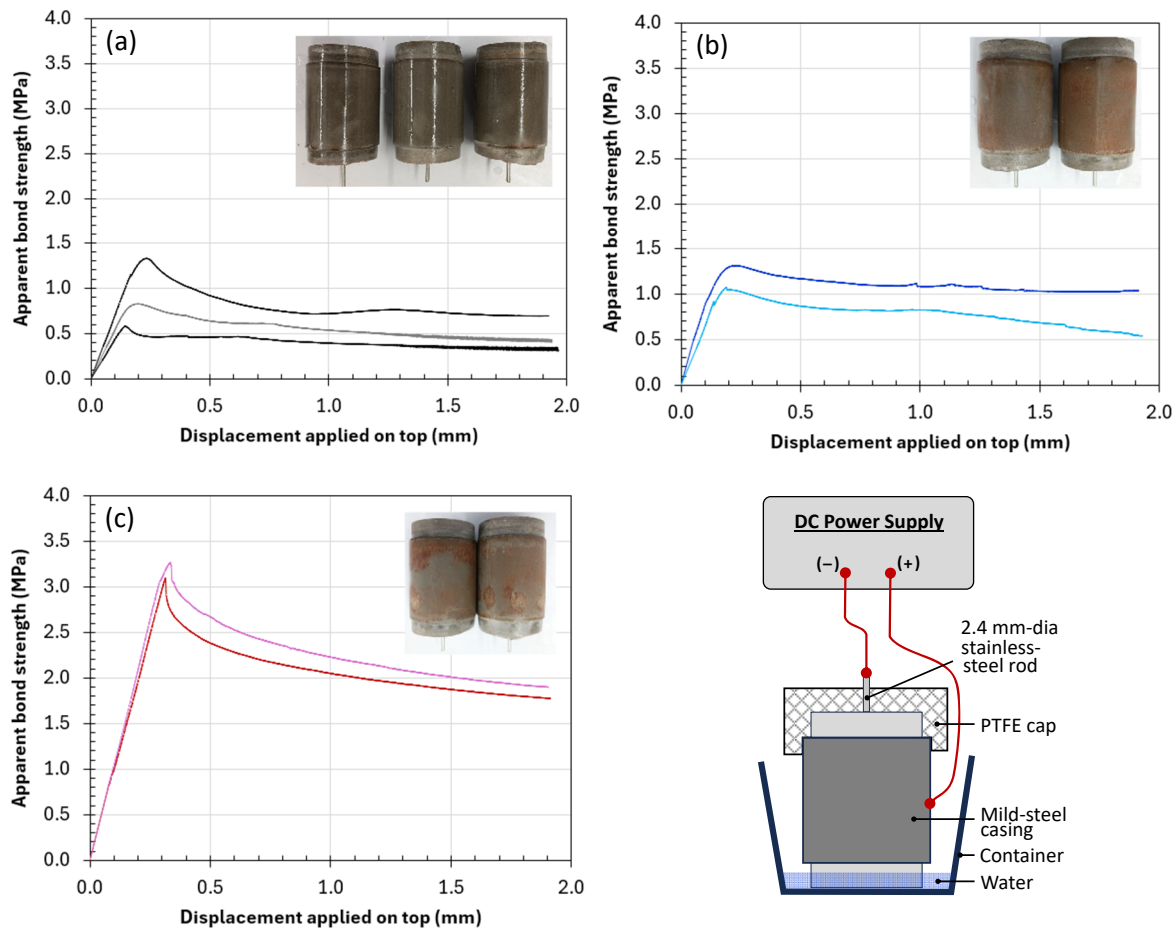


Figure 13. Results of bond test on samples exposed to accelerated corrosion.

Further evidence of the effect corrosion was obtained from the second series of CemCorr samples. For the primary sealants, it was observed that the mean bond strengths following extended corrosion exposure were consistently higher than those recorded prior to corrosion. Extensive corrosion formation was evident at the sealant/steel casing interface in all sealants, caused by the application of electrical current during the accelerated corrosion process. Sealant S2 samples demonstrated the most pronounced increase in bond strength, rising markedly from 1.51 MPa to 5.98 MPa. This significant enhancement could be attributed to the high modulus of elasticity of this sealant, which may have led to substantial internal confining stress resulting from the expansive corrosion at the interface. Sealant S4 samples, as before, exhibited the lowest mean bond strength of 0.91 MPa, yet this still represented a noteworthy improvement from its pre-corrosion value of 0.51 MPa. Sealant S1 samples displayed considerable variability in bond strength, influenced by significant differences in corrosion levels across individual test

specimens. The mean bond strength for Sealant S1 was recorded at 9.3 MPa, surpassing its previous value of 4.7 MPa. Sealant S3 samples also showed an increase, with a mean bond strength of 3.75 MPa, compared to the pre-corrosion value of 3.54 MPa. The increase was more modest, likely attributable to the lower modulus of elasticity of Sealant S3, which would result in reduced additional confining pressure.

To provide additional insights into the effect of corrosion, three additional samples were cast: two using the same mild-steel tube casing and the other using stainless-steel mould. These samples were cured at enhanced temperature and pressure. They were also tested using the same test procedures, involving sample pre-conditioning and testing temperature of 80°C. It was observed that corrosion at the interface resulted in elevated bond strength by 22–39%, further supporting the hypothesis regarding the secondary effect of corrosion on bond strength. While corrosion may temporarily elevate bond strength due to confining pressure, this effect is considered not permanent and is expected to diminish over time as the sealant undergoes creep and shrinkage. As such, the increased bond strengths measured in samples with corroded metal casing are considered artificial. Over time, the expansive nature of corrosion, combined with the sealant’s creep and shrinkage, may lead to greater porosity within the corrosive layers forming on the inner casing surface as corrosion advances. Ultimately, this porous layer could create leakage pathways. To mitigate this risk, it is strongly recommended to take preventive measure against corrosion by employing non-corrosive casings or sealants that have properties that can reduce the likelihood of corrosion initiation.

3.5 Effect of setting time

During the initial few hours after gauging, cement slurry undergoes setting i.e., increasing in rigidity and transitioning from a liquid to a solid state. Although no direct measurements of setting time were undertaken, it was observed that the setting time of the four sealants at ambient laboratory temperature varied significantly, increasing in the order: S4 (less than 30 mins) < S2 (around 45 mins) < S3 and S1 (more than 1 hour). Coincidentally, this aligns with the order of the mean bond strengths obtained from the four different sealants. Given that cement slurry with a quick setting time can be expected to solidify at a faster rate, particularly when exposed to a rapid temperature increase (simulated in this project by the relatively rapid initial temperature rise from 20°C to 80°C in 4 hours), it is postulated that a rapid state change may compromise bonding with the metal casing. Moreover, in this work, despite using high pressure (300 bar) curing, the situation is likely further exacerbated by the expansion of the metal casing during the initial heating stage and the absence of lateral confinement provided by surrounding rock formations.

In view of above, it was considered necessary to study the effect of setting time. The testing for Sealant S4 was repeated to check if the low bond strength observed was attributed to its rapid setting characteristic. Hence, in the repeat test, a retarding agent of undisclosed type and quantity was added to the original mix to slow down the initial reaction kinetics of the cement. The same test procedures, with elevated curing temperature and pressure, were implemented as previously. **Figure 14** compares the original S4 result with S4R. Beyond the 6-day point (above 110 °C) the profiles of both samples are largely similar, though S4R has slightly lower Resistance but is still within the range of variation expected between the two batches. This suggests that the inclusion of the expansive agent does not have a significant influence on the bulk properties of the sealant, particularly in terms of pore connectivity. However, the addition of the retarding agent has clearly influenced the initial profile of the electrical response, with the S4R sample displaying significantly delayed and reduced Resistance from gauging through the first 7 days, when compared to the original S4 sealant. This demonstrates the distinct effects of the retarding agent on the setting process and the resulting development of pore structure during the early stages of curing. The influence on the later stages of curing appears minimal, as reflected in the observed similarities, including the slight increase in value around the 20-day mark and the consistent final increase. This further confirms that the inclusion of the retarding agent primarily influences the early stages of hydration.

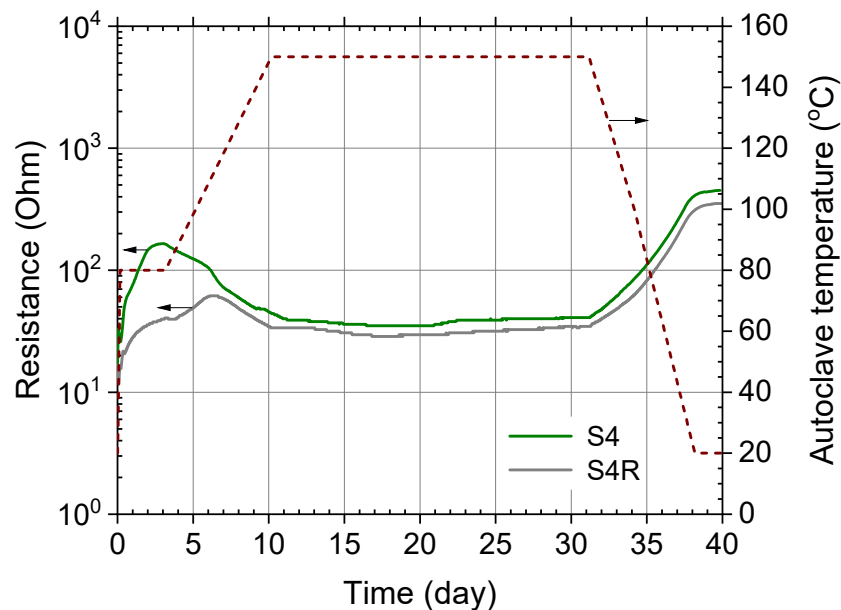


Figure 14. Resistance profile of Sealants S4 (original) and S4R (repeat with retarding agent).

Prior to bond testing, radial cracking was observed at the bottom part of the material protrusion above the casing rim, through which the bond test load is applied. This required milling of the sealant material flush with the steel casing rim, to enable load application during the bond test. The mechanism underlying the radial cracking due to the addition of expansive agent is not fully understood but might have resulted from tensile stress developed in the protrusion above the steel rim due to the restraint on volumetric changes of the sample body during curing imposed by the steel casing. **Figure 15** compares the mean bond strength obtained from this repeat test (denoted S4R) with the original test (denoted S4). It is immediately apparent that the mean bond strength of the repeat samples was significantly higher than that of the original S4 mix, averaging at 5.45 MPa, clearly highlighting the benefits of slowing down the initial reactions of cement on bonding. This corresponds to an approximately five-fold net increase once the difference in the mean bond strengths of the reference samples in the two batches has been considered. Interestingly, it was found that failure of the repeat samples was governed by crushing of the sealant face under the loading applicator instead of shear sliding at the sealant/steel interface. Following bond testing, the metal casing was split into two to get access to the sealant and inner casing surface, see **Figure 15**. Interestingly, there is a large proportion of the sealant material still strongly adhered on the steel surface, confirming the high bond strength observed. Despite this, a moderate level of corrosion, comparable to that observed in the S4 mix was evident, suggesting that corrosion is governed by the sealant characteristic itself.

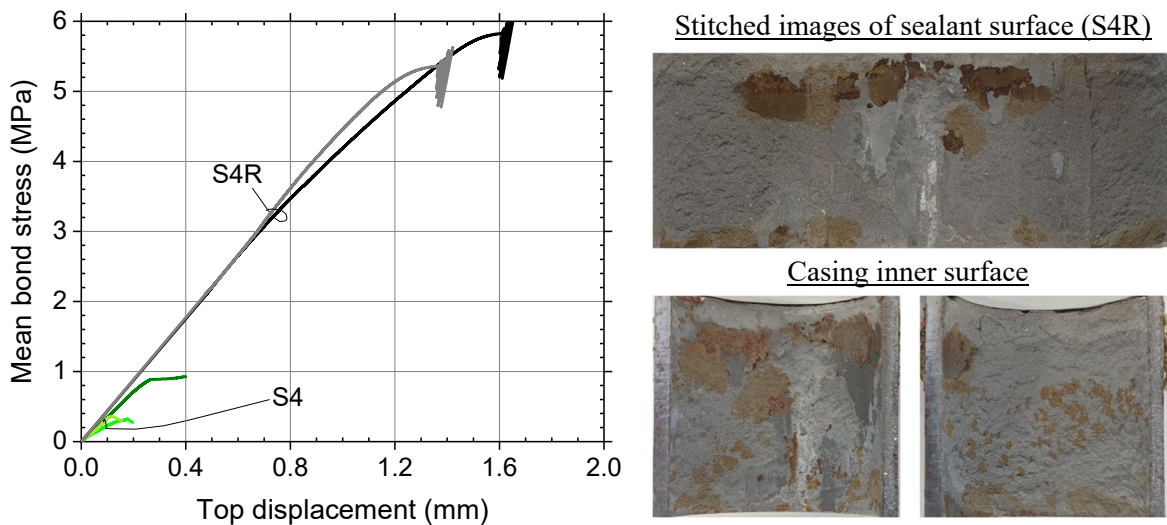


Figure 15. Bond performance of Sealant S4R with a retarding agent compared to that of reference Sealant S4 without a retarding agent, along with images of surface conditions post testing.

3.6 Effect of curing conditions

Cement hydration involves complex chemical processes that are thermally activated. The in-situ elevated temperature and pressure environment of a deep re-purposed oil or gas well should therefore be replicated in the curing and testing of CCS sealant materials as closely as possible. **Figure 16** compares the mean bond strengths obtained from test samples cured under elevated temperature and pressure (up to 150°C and 300 bar over 38 days, denoted S1 and S1R) and those cured under laboratory condition (20°C and atmospheric pressure over 28 days, denoted S1A), plotted against their respective mean compressive strengths. Note that S1R was obtained from sealant samples encased in stainless-steel, whereas S1 and S1A are from a similar sealant encased in mild steel. The beneficial effect of enhanced curing is strongly indicated by the bond and compressive strengths of samples cured under elevated conditions (S1 and S1R), compared to those cured under ambient temperature and atmospheric pressure (S1A). It is interesting to note that while enhanced curing resulted in an approximately twofold increase in compressive strength (~35 MPa to 60–75 MPa range), it resulted in four to fivefold increase in bond strength (~0.9 MPa to 3.6–4.6 MPa range). The elevated pressure used in the main curing regime (300 bars) is anticipated to enhance the densification of the pore structure of the sealant, thereby increasing its compressive strength. Additionally, the elevated pressure can minimise volumetric changes (e.g. shrinkage). These two factors contribute positively to bond strength, explaining the more pronounced improvement observed in the overall bond strength, see **Figure 16**.

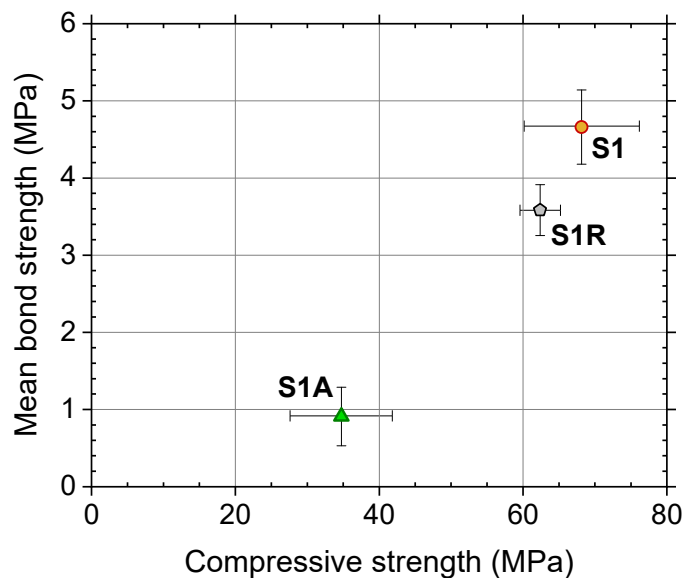


Figure 16. Key properties of Sealant S1 cured under ambient and elevated curing.

3.7 Bond strength of non-Portland based sealant

Sealant S5 was the only sealant studied in this project that did not contain Portland cement. As the development of this mixture took place during the initial phase of the project, the fabrication of samples for this series of testing suite commenced in the latter half, during the final testing phase in this case. At this stage, it was deemed essential to produce samples of Sealant S5 alongside Sealant S1RF (repeat final) as a reference. During this process, consideration was given to utilising both mild-steel and stainless-steel casings. Because of the considerable differences in the fundamental compositions of the sealant materials, the curing process for the two sealants was conducted in separate chambers to prevent possible cross-contamination. This precaution was considered necessary as Sealant S5 contained a high concentration of alkali activator, and this could significantly accelerate the hydration reactions of Portland cement and other supplementary materials in the mixture. These test samples underwent identical fabrication and curing processes as the other four sealants, along with the same pre-conditioning and testing protocols.

Figure 17 displays the mean bond stress plotted against displacement, using the same data presentation as before. Sealant S5 samples achieved a mean bond strength of 10.2 MPa regardless of the casing materials used (e.g., mild steel or stainless steel), whereas the bond strengths of the repeat S1RF samples ranged from 8.76 to 10 MPa, averaging 9.4 MPa. These values were more than twice the average bond strengths recorded in previous batches and exceeded figures reported in published literature. The reasons for this increase were not clear, but several factors may have contributed. Potential causes include inconsistencies during the oil removal process in the preparatory stage or errors in material batching. In the case of the latter, this may include, for instance, the accidental addition of a retarding agent (which has previously been shown to enhance bond strength) or the unintended use of an expansive agent during material batching. Furthermore, issues arising during transportation from Norway to the UK could also be a factor, although such complications would typically be expected to reduce bond strength rather than enhance the value.

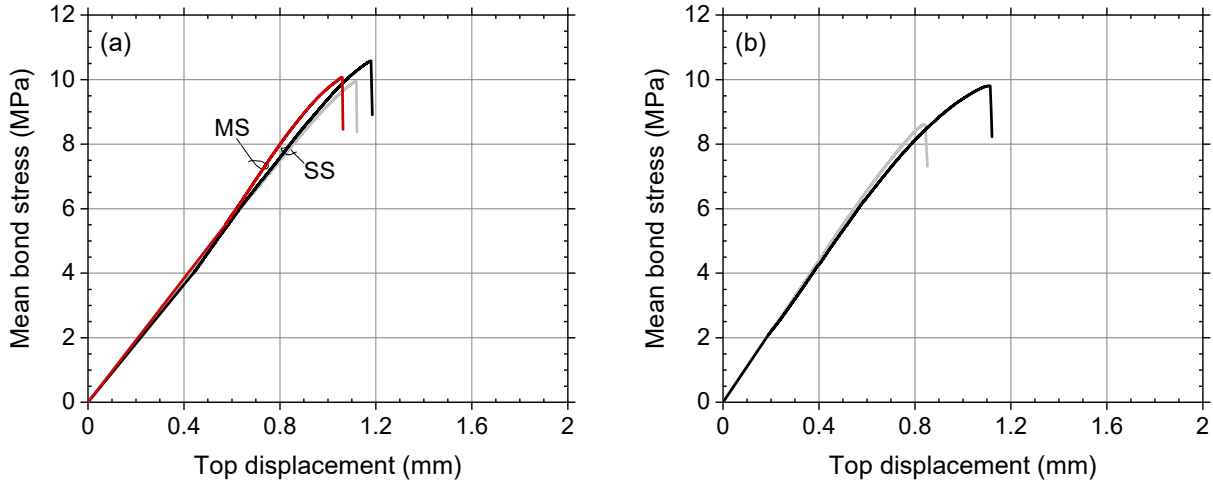


Figure 17. Bond performance of: (a) Sealant S5 and (b) Sealant S1RF (repeat).

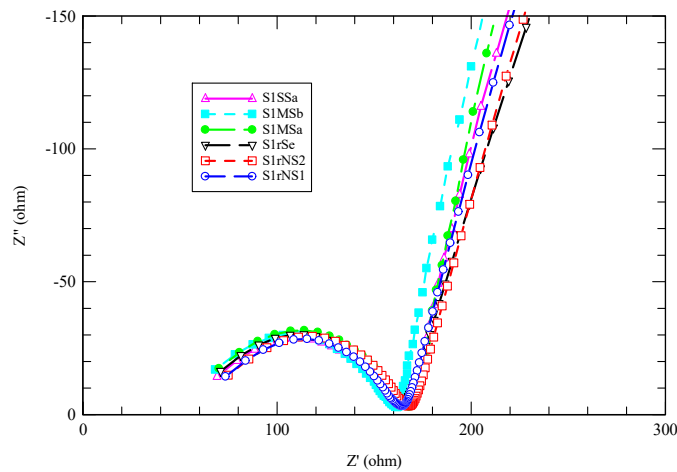


Figure 18. Comparison of the Impedance response of Sealants S1 (first 3 data sets) and S1RF (second 3 data sets).

To examine the aforementioned issue further, impedance measurements were conducted on the test specimens prior to undertaking the bond testing. The findings, illustrated in **Figure 18**, demonstrate a consistent response, suggesting that the bulk electrical properties remain fundamentally unchanged across the samples between the two batches. Therefore, any discrepancies observed are likely to be due to factors relating to the sealant-casing interface. This could be due to the unintentional presence of an

expansive agent, which might have inadvertently occurred during material batching. It is worth noting that the presence of such an admixture may not be reflected in the impedance measurement results.

Figure 19 (a) displays the surface conditions of the Sealant S5 samples, showing both the outer surface of the sealant and the inner surface of the steel casing. Notably, the particular sealant exhibits a remarkably smooth interface with the steel casing, exhibiting minimal and largely no visible signs of corrosion with the exception of only at a small, localised area as shown in the Figure. Among the various sealants tested in this project, this sealant displays the smoothest surface, effectively replicating the texture of the internal surface of the steel casing. A noticeable layering effect can also be seen, which is indicative of material segregation during the fabrication of the samples. This is likely attributable to its less viscous property compared to the other sealants tested in this study. The upper sections of the samples display lighter colour covered with numerous white spots, while the lower sections display a darker colour, also covered with several white spots.

For comparative purposes, **Figure 19 (b)** displays the surface conditions of the Sealant S1RF samples, both on the exterior surface of the sealant and the inner surface of the steel casing. Interestingly, there are also no visible signs of corrosion, which contradicts the results from the previous three batches. It is noteworthy that in this batch, the material near the surface has sheared off, leaving white zones adhered to the steel surface, suggesting that this layer must have separated under the application of shear load. This observation implies that the bond failure of the S1RF samples is due to material failure beneath the steel/material interface instead of debonding. While the exact cause of the difference could not be determined due to the use of a proprietary mix, the lack of corrosion in this set of samples could be attributed to enhanced volumetric stability compared to the original S1 sealant produced in previous batches.



(a)



(b)

Figure 19. Conditions of the sealant's outer surface of and the pipe's inner surface following bond testing: (a) Sealants S5 and (b) S1RF.

3.7 Non-destructive testing

3.7.1 Post enhanced curing

During the post-curing stage, impedance spectra for all sealants were obtained using a Solartron 1260 Impedance Analyser. These measurements were carried out on samples with both parallel 2-pin and

coaxial 1-pin sample types, which had cured in a water medium within the autoclave. Data were acquired using a 1 Volt peak-to-peak excitation voltage across a frequency range of 1 Hz to 10 MHz at 10 logarithmically spaced points per decade of frequency increase. The frequency analyser and a connected sample are shown in **Figure 20**.

From parallel measurements, the value of k , the sample-electrode geometric parameter, was established for both the coaxial and parallel 2-pin sample configurations by comparing the impedance results from each with those from the Perspex cube sample holder. The values obtained for the coaxial and two-parallel pair electrode configurations were, $k_{1p} = 0.1568$ and $k_{2p} = 0.1046$ /m.



Figure 20. Solartron 1260 Impedance analyser with coaxial sealant sample.

The processed Impedance results for Sealants S1 to S5 are presented below in **Figure 21** in Nyquist diagram format, with Reactance plotted as a function of Resistance as frequency increases from 1Hz to 10MHz. The plots for S1, S2 and S3 show a visually similar pattern proceeding from right to left as frequency is increased. This is essentially a long spur/tail, and a shallow arc conjoined at a *cusp point* where the Reactance reaches a minimum value. Superficially, this is the same pattern shown by plain OPC. The right-hand tail (low frequency section) of the response is determined not simply by the sample material properties but largely by the interaction of the material and electrodes at their interface. In the case of the coaxial configuration this includes the sealant/casing interface. It is observable that the absolute impedance values as well as the frequency characteristics of this part of the response are

distinguishable for each sealant. They are also distinguishable between electrode type – particularly for Sealant S5.

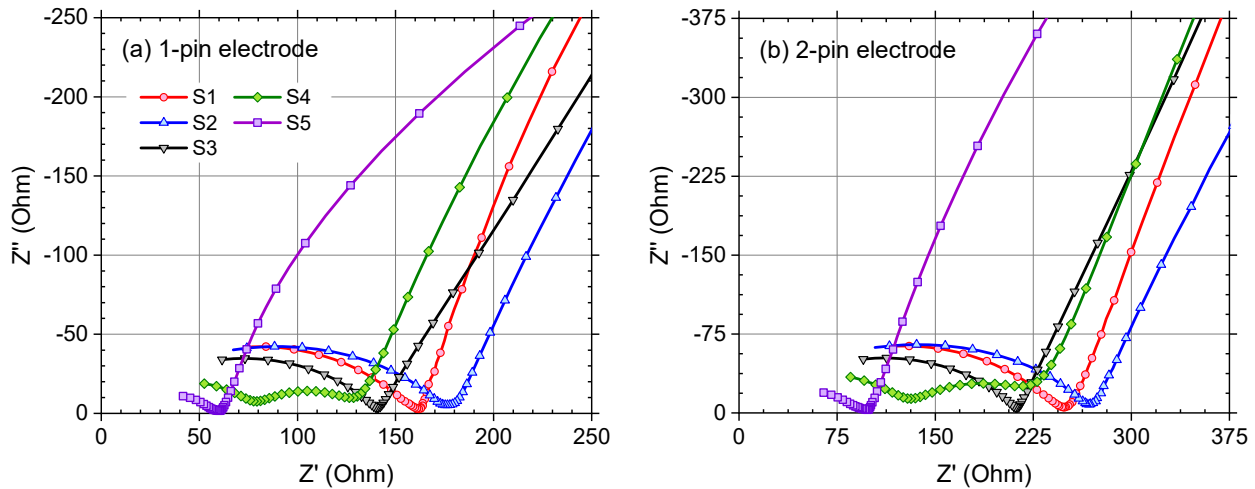


Figure 21. Post-curing Impedance plots of Sealants S1–S5.

Of interest is the Impedance response of Sealant S4, in that it reveals a dual-arc feature instead of a single-arc feature, as displayed by the other four sealants. It is notable that this sealant is derived from a different cementitious material (calcium aluminate) and contains several undisclosed proprietary additions. Similar Impedance features have previously been observed in OPC based materials containing supplementary additions.

Tables 2 and 3 present significant parameters discernible on the Impedance response of each sealant for the coaxial electrode configuration or parallel 2-pin electrode configuration. These are:

- (i) The frequency at which Reactance is at a minimum
 - This location is referred to as the cusp point, effectively dividing the bulk material response on the left-hand side of the response from the material/electrode interface response on the right-hand side.
- (ii) The Resistance at the Cusp frequency
 - This parameter is generally regarded as the true bulk properties of the sealant material.
- (iii) The Conductivity at the Cusp frequency
 - This is the reciprocal of (ii) and hence this parameter can also provide an approximation of the direct current Conductivity of the sealant material.

Table 2. Significant parameters in Coax Impedance plots.

Sealant	Cusp Frequency, kHz	Cusp Resistance, Ohm	Cusp Conductivity, S/m
S1a	4	167.9	0.0380
S2c	5	178.8	0.0357
S3b	10	140.7	0.0453
S4b	5, 250	126.6, 93.5	0.0504, 0.0682
S5b	10	61.3	0.1041

Table 3. Significant parameters in 2-Pin Impedance plots.

Sealant	Cusp Frequency, kHz	Cusp Resistance, Ohm	Cusp Conductivity, S/m
S1b	6.3	249.0	0.0384
S2a	7.9	268.1	0.0357
S3b	10	212.4	0.0450
S4a	5, 250	190.5, 136.2	0.0502, 0.0702
S5a	10	98.2	0.0974

The Resistance at the cusp frequency can usually be taken as indicative of the true bulk value at zero frequency. Note, however, the dual cusp effect in the Sealant S4 response occurs at relatively low and high frequencies, and hence it is possible that the true bulk Resistance lies somewhere on the middle arc, complicating interpretation. The Conductivity can be calculated from an impedance measurement via the following equation,

$$\sigma(\omega) = \frac{Z'(\omega)}{Z'(\omega)^2 + Z''(\omega)^2} \frac{1}{k} \quad \text{Eq. (2)}$$

where $Z'(\omega)$ is the real component of impedance (resistance) and $Z''(\omega)$ is the imaginary component of impedance (reactance).

Figure 22 presents the frequency dependent conductivities of each sealant derived from both electrode configurations. The solid data point indicated on each plot is the cusp frequency point that gives the direct conduction value of conductivity. It is evident that the conductivity of the sealants varied, increasing in

the order of $S2 < S1 < S3 < S4 < S5$, with values ranging from 0.036 S/m to 0.010 S/m, see **Tables 3 and 4**. Conductivity is, however, influenced by the pore-fluid conductivity, which can affect the bulk conductivity value, although this is not expected to differ significantly among the three OPC-based sealants. Considering the bulk conductivity values of these three sealants, Sealant S2 is anticipated to be less permeable than Sealant S1, whereas Sealant S3 is likely to be more permeable than Sealant S1. Due to the presence of chemical activators (alkali), Sealant S5 is expected to have a significantly higher ionic content which is likely to have elevated its pore-solution conductivity (e.g., studies have suggested 2-3 times higher), thereby resulting in a higher overall conductivity. Due to the absence of the pore-fluid conductivity data, this makes it difficult to ascertain the relative permeability of this sealant compared to the other sealants. Lastly, the higher conductivity of Sealant S4 indicates that it is more permeable than the OPC-based sealants.

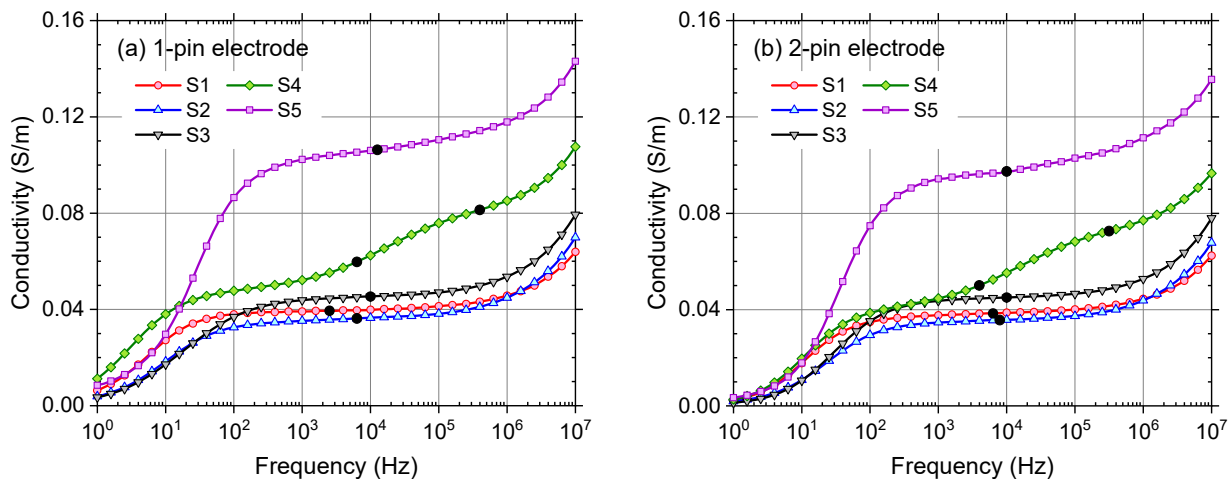


Figure 22. Post-curing Conductivity plots of Sealants S1-S5.

3.7.2 Post exposure: Effect of corrosion

Figures 23(a) and (b) illustrate the impedance response measured across all LabCorr samples over the frequency range of 1Hz to 10MHz. The Plots shown in **Figure 23(a)** represent the response obtained 18 days after casting before the application of current, whereas the Plots shown in **Figure 23(b)** correspond to the response from 18 days to 83 days, with the current being activated from Day 26 onwards. It should be noted that in these plots, no nulling of lead-inductive effects has been performed over the full frequency range. As can be seen from **Figure 23(a)** that all samples exhibit a comparable response, characterised by a spur at the low-frequency end of the curve (forming part of a larger arc) and a bulk response at the high-frequency end. The spur represents the behaviour at the sample/sealant interface,

which is of particular interest. At this stage, there is no evidence of any additional polarising layer effect at the low-frequency end due to exposure to corrosion.

Regarding the Plots shown in **Figure 23(b)**, it is evident that for samples exposed to zero current (left-hand-side plot), the impedance spectra showed a consistent shift to the right, suggesting continued hydration. No significant alterations to the spur at the low-frequency end of the curve were observed. In samples subjected to a 15mA current (middle plot), a similar trend is evident, although there are noticeable changes in the radius of the spur at the low-frequency side of the curve, which may indicate corrosion occurring at the sample/sealant interface. For samples exposed to a current of 30mA, a more significant to the right is observed, suggesting that prolonged exposure to the current influences not only the sample/casing interface but also accelerates the cement hydration process. This could account for the previously observed increase in apparent bond strength, see **Figure 13**.

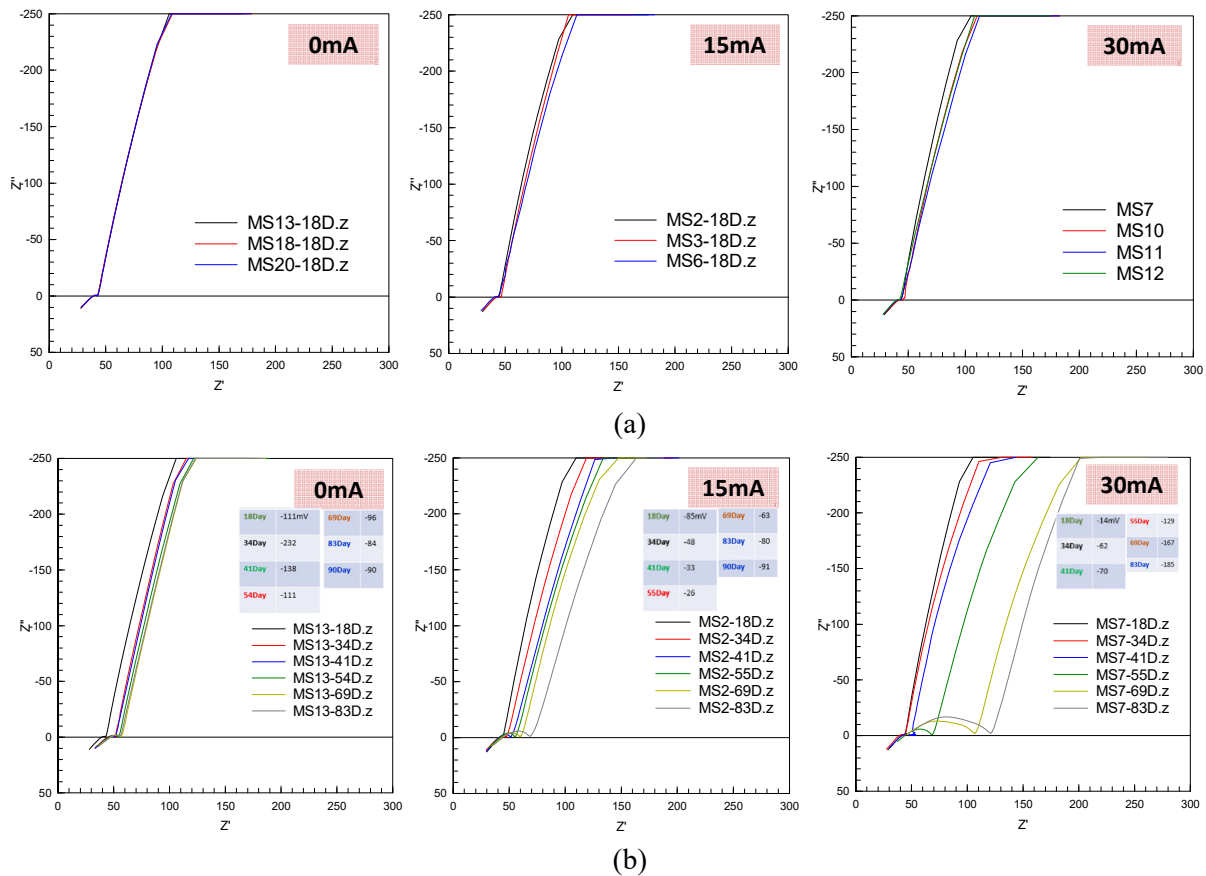


Figure 23. Impedance response for (a) Day 18 and (b) Days 18 – 83 (no nulling).

Figure 24 presents the impedance response for all samples tested on Day 83. It is apparent that prolonged exposure to corrosion has significantly influenced the overall response. Notably, the samples subjected to the high current of 30mA show a considerably wider variation in their impedance spectra compared to those exposed to lower current levels or no current at all. This increase in variations may be attributed to the inherently variable nature of corrosion processes. Post-testing sample extraction showed that the corrosion tends to progress more unevenly, leading to greater variations in the degree and distribution of corrosion across the samples (see **Figure 13**).

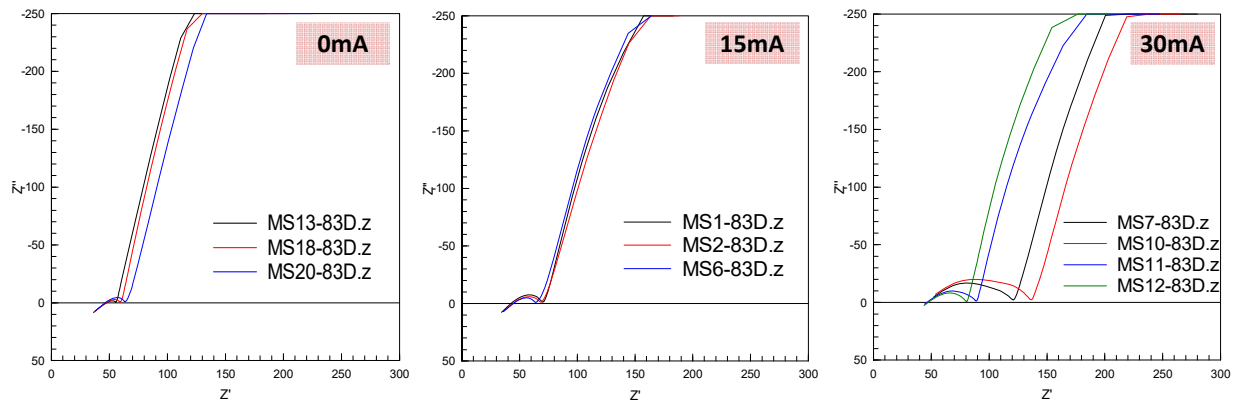


Figure 24. Impedance response for Day 83 for all test samples (no nulling).

To obtain a better understanding of the influence of prolonged exposure to corrosion, **Figure 25(a)** illustrates the response of three individual sample exposed to no current, 15mA, and 30mA current levels throughout the entire exposure period, with a summary of the bulk resistance for the three representative samples presented in **Figure 25(b)**. As previously mentioned, the applied current levels correspond to current densities of 0, 0.21, and 0.42 mA/cm², respectively. The results show that all samples exhibited distinct responses depending on the current level applied. The low-frequency region of the curve forms part of a much larger arc and represents the response primarily at the sample/sealant interface and is therefore of particular interest. All samples displayed a progressive shift to the right-hand side of the curve, which can be attributed to the self-curing of the sealant. For samples subjected to prolonged exposure to electrical currents, a much more pronounced shift was observed, potentially attributed to additional curing effects caused by the application of electrical current, which is required to drive the corrosion process. In general, three distinct stages of response were observed: (i) an initial region of increasing resistance due to curing, (ii) a transitional region where resistance increased further, likely due to a combination of additional curing effects and corrosion at the steel casing/sealant interface, and (iii)

a final region where resistance continued to increase, driven primarily by further curing effects and likely corrosion at the interface. The observed increase in bulk resistance would suggest that the application of electrical current must have enhanced cement hydration, which may have contributed in part to the previously observed increase in apparent bond strength (see Figure 13).

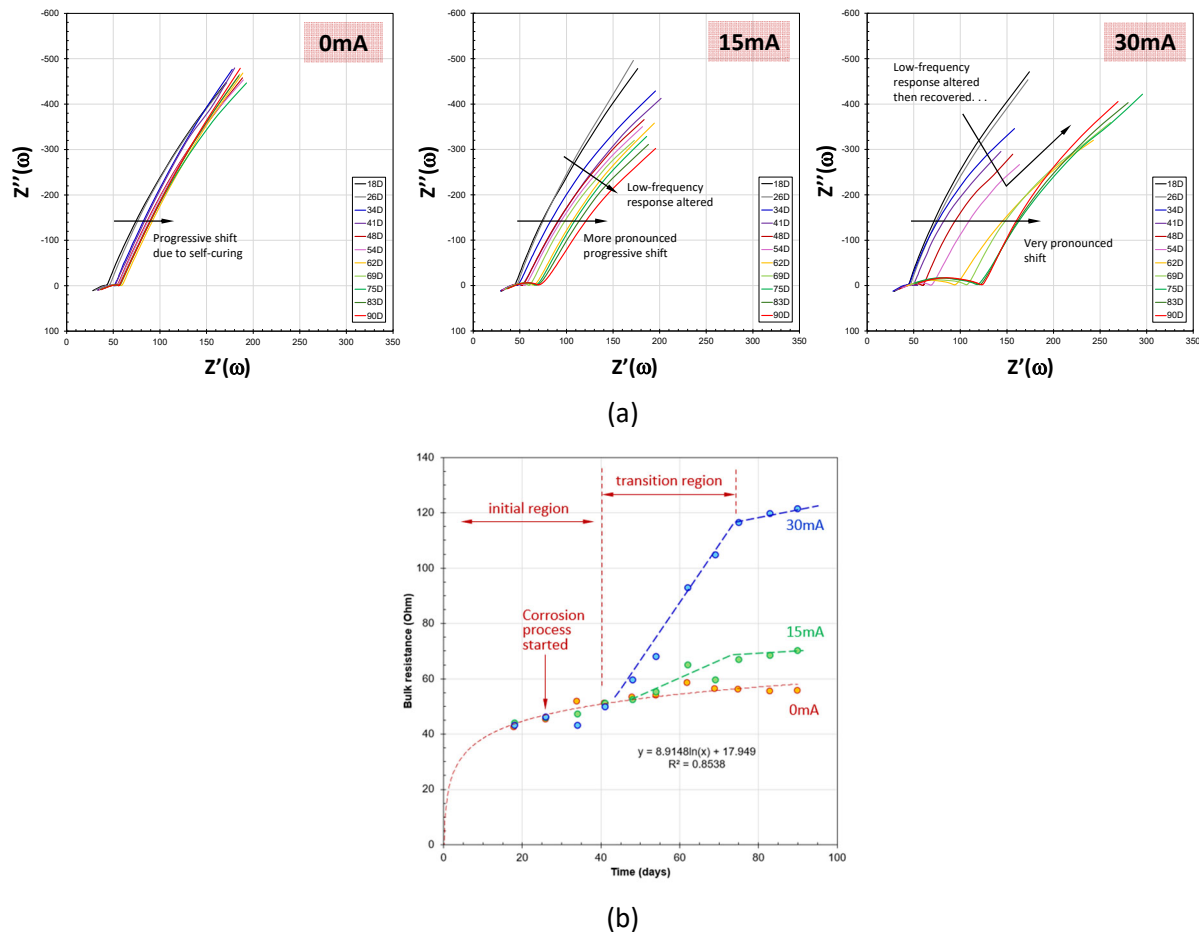


Figure 25. Influence of exposure to prolonged corrosion on impedance and bulk resistance.

In addition to influencing the resistive component, corrosion at the steel casing/sealant interface is anticipated to introduce capacitive effects to the overall system. This is attributed to the development of corrosion products at the sealant/steel interface, which possess distinct properties that can alter the electrical characteristics of the system. To investigate this phenomenon, electrical circuit analysis was performed by modelling the low-frequency portion of the impedance spectra using an equivalent circuit comprising a resistor and capacitor connected in parallel. The low-frequency range was deliberately selected, as this region effectively captures the behaviour at the sealant/steel casing interface, where the

effect of corrosion is expected to be the most prominent. An example of the circuit parameters obtained from this analysis is shown in **Figure 26(a)**. As can be seen, both the resistive and capacitive components of the equivalent circuit were influenced by the prolonged induced corrosion, indicating that corrosion at the sealant/casing interface not only alters the interface characteristics but also impacts the overall response.

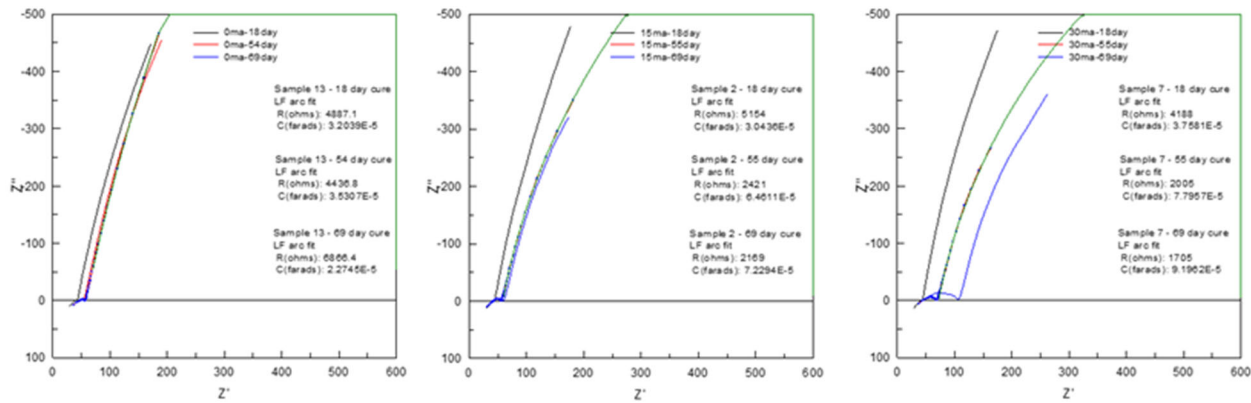


Figure 26. Equivalent circuit modelling on the low-frequency response.

Figure 27 displays the impedance response of autoclave-cured Sealant S1-S5 samples subjected to both high-temperature curing and corrosion regimes. Based on earlier measurements, the current was initially set at 30mA. However, after 2 days, this was further reduced to 20mA and subsequently switched off after 7 days, as the voltage in several samples approached the upper limit of the power supply. This would suggest that high-temperature exposure significantly increased the likelihood of corrosion initiation, with the rapid increase in voltages suggesting that corrosion progresses more rapidly at the sealant/casing interface than the lab-cured samples. The current application was then resumed at 5mA starting from Day 14. From **Figure 27**, it is interesting to note that all sealants produce a significantly different impedance response at the beginning of testing (Day 0). The impedance spectra of the sealants at Day 14, post initial corrosion regime, are comparable to those measured at the start of experiment (prior to current application), particularly on the shape and extent of the high-frequency bulk arc. This would indicate that there was virtually no additional curing and could be associated with the fact that this series of samples was subjected to the enhanced curing regime (elevated temperature and pressure). It is however interesting to note that the spur at the low-frequency end showed notable changes, which is generally much shorter.

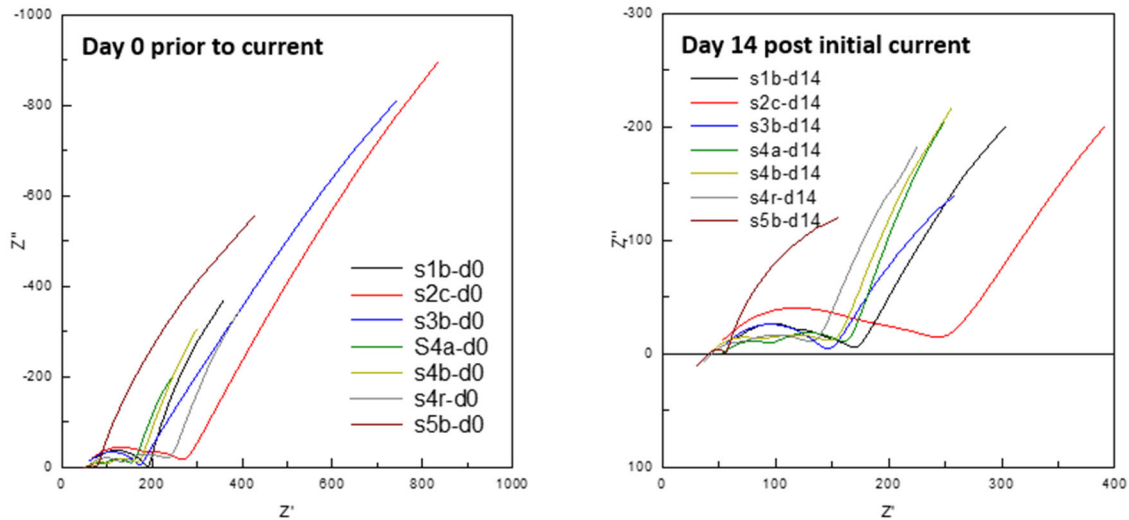


Figure 27. Impedance response of Sealants S1-S5 before and after exposure.

3.7.3 Effect of temperature

The impedance measurements discussed earlier were undertaken at a controlled laboratory temperature of 20°C and under ambient pressure. In order to provide insights into the influence of temperature and pressure on the relative bulk permeation properties of the sealants, samples of Sealants S1 to S5 (including Sealant S4R) were fabricated and exposed to varying temperatures ranging from 20°C and 150°C range under a pressure of 300 bars. These samples were initially subject to 150°C for a period of up to 31 days, after which the temperature was gradually reduced to 20°C in 7 days, at a rate of approximately 0.77°C per hour. During this temperature changes, the Resistance of the samples were continuously monitored using a bespoke data logger, which recorded 2 measurement data per hour.

Figures 28(a) and (b) present the measured resistance over a 7-day period, with (a) displaying the complete dataset for the five sealants and (b) providing a magnified view for the four sealants. It is evident that the bulk Resistance of all the sealants increases significantly, displaying a highly nonlinear response as the temperature decreases from 150°C to 20°C. Due to the elevated curing, the cement hydration and other associated reactions can be assumed to have effectively ceased, and that the ionic concentration within the pore fluid to also have stabilised. Hence, the marked rise in resistance can be attributed solely to the effects of temperature. These effects arise from the reduced mobility of ions within the pore structure of the sealant body, as the temperature decreases, thereby causing the overall increase in bulk Resistance.

To gain a clearer understanding of the temperature effect, this temperature-dependent behaviour is represented in the Arrhenius format, viz,

$$R = R_0 e^{\left(\frac{E_a}{R_g T}\right)} \tag{Eq. (3)}$$

where R (Ohm) is the electrical resistance of the sealant measured at temperature T (Kelvin); R_0 is a pre-exponential factor, representing the nominal value at infinite temperature; E_a is the activation energy for ionic conduction in cement matrix (J/mol), R_g is the Universal Gas constant (8.31446 J/(mol.K)). Equation (3) can be converted into a simple linear form by applying the natural logarithm to both sides, resulting in

$$\ln R = \frac{E_a}{R_g} \left(\frac{1}{T}\right) + \ln R_0 \tag{Eq. (4)}$$

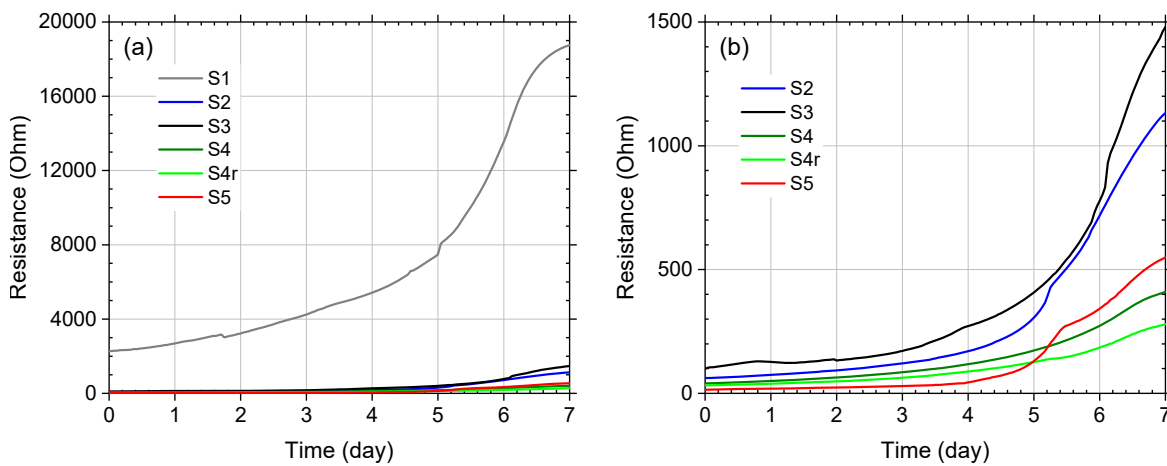


Figure 28. Resistance of Sealants S1-S5 measured over a temperature range of 20-150°C within a 7-day period.

Figure 29 (a) presents the plots of the natural logarithm of bulk Resistance ($\ln R$) for each sealant plotted as a function of $1000/T$. It is interesting to note that the highly nonlinear curves observed earlier have transitioned into less nonlinear response, with a linear relationship emerging over certain temperature ranges. Interestingly, Sealants S4 and S4R display a predominantly linear response across the entire temperature range $150^\circ\text{C} \rightarrow 20^\circ\text{C}$. Building upon the linearity of Equation (3), determining the slope of each curve over a certain temperature range can provide useful information. The slope can subsequently be multiplied by R_g to calculate the activation energy, expressed in kJ/mol. The activation energy, in this context, can be interpreted as the energy barrier that ions must overcome to enable conduction within the pore network. Hence this parameter offers valuable insights into the pore connectivity of the individual sealants. A constant activation energy across a certain temperature range would indicate that

ionic conduction through the pore network is the prevailing mechanism, with no physical alterations in the connectivity of the pore structure. To this end, the activation energy was evaluated between 80°C and 120°C, corresponding to the typical operational temperature of a well. **Figure 29 (b)** provides an example for Sealant S2, with the data point fitted using a linear equation. The activation energy values recorded for all sealants within this temperature range were largely comparable: 16.73 kJ/mol, 17.13 kJ/mol, 17.03 kJ/mol, 17.39 kJ/mol, and 14.30 kJ/mol for Sealants S1 through S5, respectively. Sealant S5 displayed a notably lower value, which could be attributed to its higher ionic content. Notably, there are specific temperature ranges below 80°C where an increase in slope is evident as temperature decreases. Although this temperature range currently falls outside the primary area of interest at present, this approach could be further explored to assess how pore connectivity for a particular sealant changes with variations in temperature.

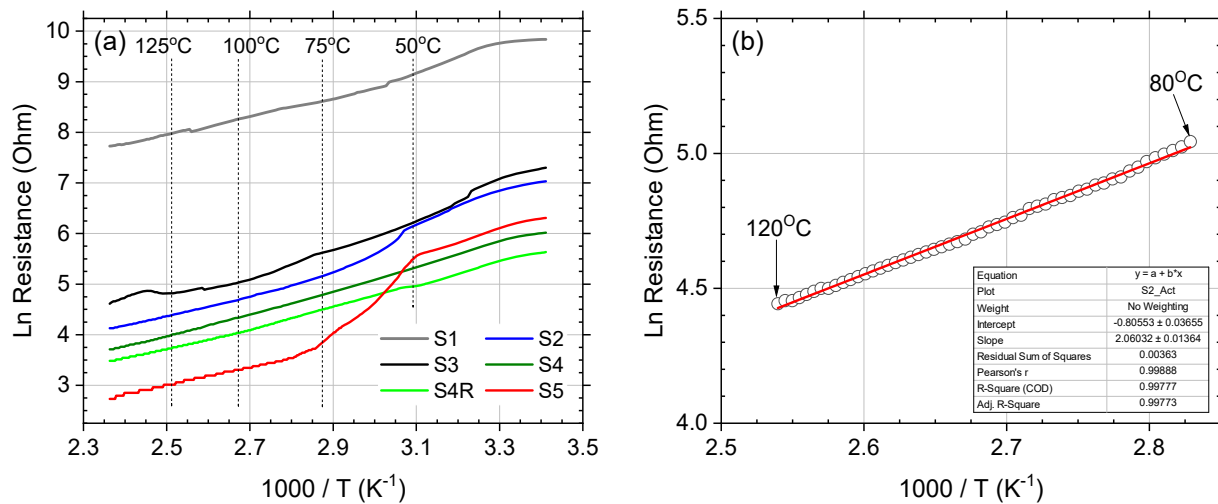


Figure 29. Arrhenius plots for: (a) Sealants S1-S5 over the temperature range 20-150°C and (b) Sealant S2 over the temperature range 80-120°C.

3.8 Comparison between properties

In this section, the data obtained from both the shear-bond testing and electrical measurements are compared. The parameters of interest include the compressive strength of the sealants, shear bond strength, and characteristics related to bulk resistance and capacitance. Furthermore, permeability is also taken into account in this analysis, as it offers an interesting comparison with the bulk resistance values obtained from the different sealants, which represent the connected porosity of the sealants, as previously discussed.

Figures 30(a) and **(b)** illustrate the observed relationships between the evaluated parameters between the mechanical properties obtained from shear-bond testing and electrical measurements. With reference to **Figure 30(a)**, there appears to be a notable correlation between bulk resistance and compressive strength, which is somewhat unexpected. Bulk resistance typically indicates the level of connected porosity within the sealant, while compressive strength is indicative of the overall structural integrity of the pore network. The apparent correlation between these parameters is interesting and warrants further investigation. In contrast, as shown in **Figure 30(b)**, the comparison between bulk resistance and mean bond strength reveals only a weak correlation. It is important to highlight that Sealant S4 experienced premature failure, which could have skewed the perceived trend. When the analysis is restricted to Sealants S1 to S3, the relationship between bulk resistance and mean bond strength seems to flatten, presenting a horizontal trend. This would indicate that there is little to no correlation between these two parameters. The lack of correlation can be attributed to the different characteristics these parameters represent. Bulk resistance measures the overall bulk properties of the material, such as its porosity and connected pathways. On the other hand, mean bond strength is primarily determined by the interfacial properties at the sealant/casing interface. This distinction emphasises that the mean bond strength cannot be estimated from the bulk resistance.

The correlation between the parameters obtained from the equivalent circuit modelling and mean bond strength is presented in **Figures 31 (a)** and **(b)** for samples subjected to no current, 15mA, and 30mA (current densities of 0, 0.21, and 0.42 mA/cm², respectively). Overall, it was found that the application of the electrical current not only facilitates corrosion at the sealant/sample interface but also influences the hydration and curing processes. As can be seen from **Figure 31 (a)** that there is a strong correlation between bulk resistance and the mean bond strength, and this could be attributed to the additional curing effects caused by the application of electrical current, which is required to drive the corrosion process discussed above. Interestingly, the data also show a substantial increase in the capacitive component when correlated with the mean bond strength across the various samples. This observation suggests that the capacitive behaviour may serve as a valuable indicator for monitoring the likelihood of corrosion initiation at the sealant/casing interface. The capacitive component, reflective of the changes occurring at the interface, provides further insight into the effects of corrosion and could have broader implications for detecting corrosion initiation at the sealant/casing interface.

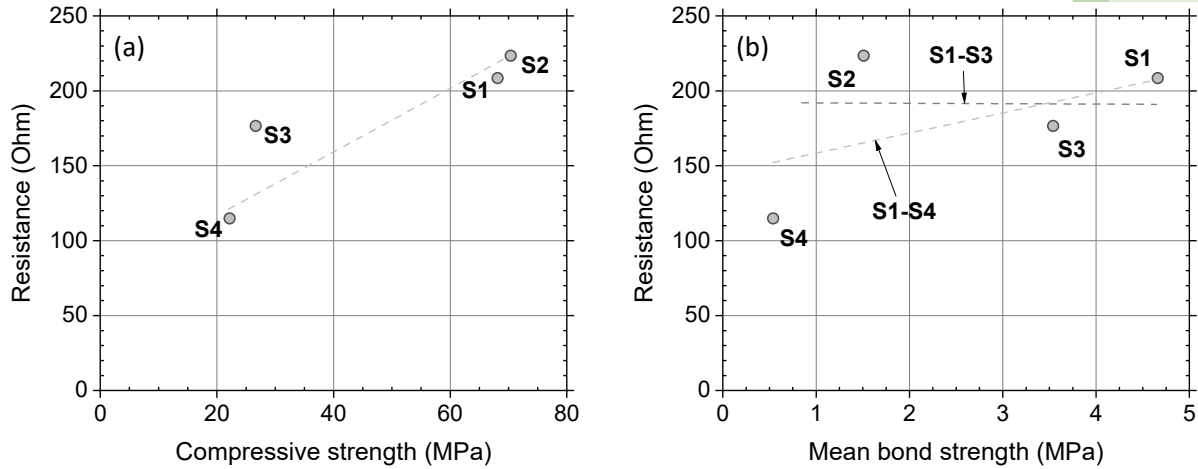


Figure 30. Comparisons of bulk resistance with measured compressive and mean bond strengths.

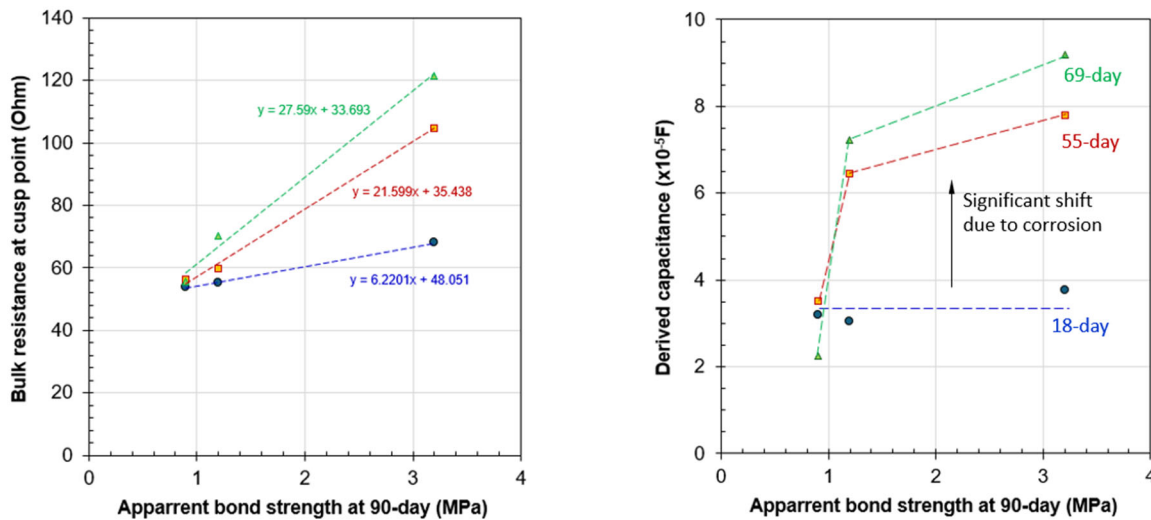


Figure 31. Comparisons of bulk electrical properties and mean bond strength after exposure.

With regards to the bulk electrical properties, **Figure 32** illustrates the conductance (the reciprocal of bulk resistance) calculated from the impedance data, plotted against the water permeability measurements of unexposed reference samples reported by our project partner in Work Package 1. For the three PC-based sealants (Sealants S1–S3), it can be assumed that the pore fluid compositions are broadly similar to allow for a direct comparison. In contrast, for Sealant S5, the pore fluid is expected to exhibit a significantly higher ionic strength due to the activators incorporated into this material (a value of two to three times has been reported in previous studies). For Sealant S4, the pore fluid composition may also differ. Additionally, Sealant S4 has a more complex frequency-dependent behaviour which makes it more difficult to determine an accurate conductivity based on the available data.

Overall, **Figure 32** displays that there is a somewhat correlation between conductance and permeability, with the conductivity increasing with increasing permeability as one would expect. Interestingly, Sealant S4 demonstrates relatively low conductance in relation to its permeability, potentially due to a lower ionic strength in the pore fluid. Conversely, Sealant S5 exhibits comparatively high conductivity relative to its permeability, which may indicate that its pore-fluid conductivity might be much higher than that of the PC-based materials (i.e., Sealants S1–S3). From the spread of the data, it appears that the pore fluid conductivity in this sealant is approximately twice that of the PC-based sealants, which broadly aligns with findings reported in published literature. The findings presented suggest that electrical measurements could offer a means of evaluating seal permeability, provided those factors influencing electrical impedance, such as pore fluid composition, are properly accounted for.

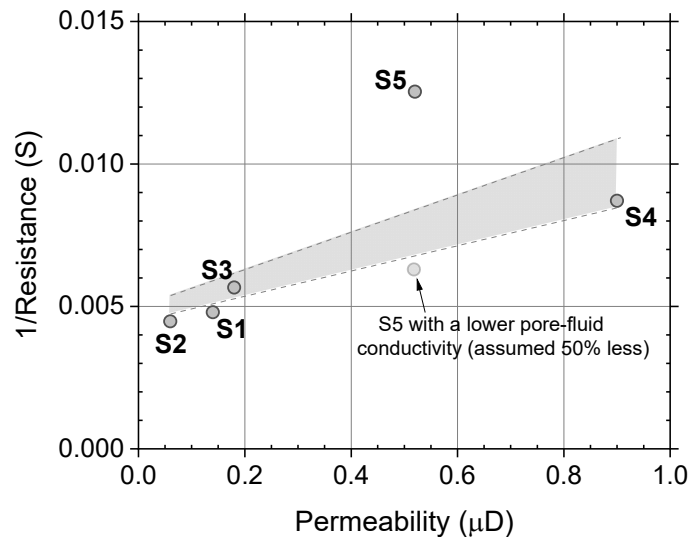


Figure 32. Comparisons of bulk conductance and material permeability.

4. Concluding Remarks

As part of the CEMENTTEGRITY project, laboratory investigations involving shear bond tests and electrical measurements were undertaken to evaluate the performance of five distinct sealants encased within cylindrical steel casing. Samples were cured under two conditions: standard laboratory conditions at approximately 20°C and elevated temperature (up to 150°C) and pressure (300 bar) to replicate the conditions typical of deep offshore CCS wells. From the results presented, the following remarks can be made:

1. A custom sample holder, designed as a miniature representation of a plugged well-bore and incorporating a steel casing, PTFE caps, and a newly designed electrode arrangement, was developed for the shear-bond and electrical testing of five proprietary sealants. The design was specifically tailored for an enhanced curing regime, capable of withstanding elevated temperatures of up to 150°C and pressures of up to 300 bar. The updated design has proven to be robust, effectively eliminating radial cracking observed in the original design during the enhanced curing process.
2. The shear bond strengths of cementitious sealants are influenced by a range of factors, with curing conditions, sealant setting time, and corrosion at the interface between the sealant and steel casing emerged as the dominant factors. Compressive strength was found to influence bond strength, but it did not guarantee good bonding performance, as evidenced by the result obtained from Sealant S2 samples.
3. Bond strengths of the tested sealants with steel casing varied quite significantly, ranging from 0.54 MPa for Sealant S4 to 4.66 MPa for Sealant S1. Of the initial four sealants, Sealant S3 displayed superior bond strength despite its moderate compressive strength. Sealant S1 exhibited elevated bond strength as a result of corrosion at the sealant/casing interface. Sealant S4 exhibited premature failure due to its rapid setting characteristics. The use of retarding agent has proved useful to enhance the bond strength of this sealant. Sealant S1R (Repeat) and S5 samples displayed more than double the bond strengths, but the reasons for this significant increase were not clear and could potentially involve a few factors such as errors in the preparatory stage or during material batching.
4. Corrosion levels varied among the test sealants, being most pronounced in Sealant S1 samples. Sealants S3 and S5 exhibited the lowest corrosion levels, while Sealant S4 exhibited moderate levels in both the initial and repeated tests, with higher bond strength observed in the latter. Sealant S5 displayed the smoothest de-bonded interface, replicating the inner surface of the metal casing.
5. The mean bond strength following corrosion was generally higher, but this enhancement is considered artificial and likely to diminish with time due to creep and shrinkage of the sealant matrix. Hence, bond strength measured in the presence of corrosion should not be used as a performance indicator.
6. The elevated curing temperature and pressure used in this study significantly improved both the shear-bond and compressive strengths of the sealants. High curing pressure was particularly effective in minimising volumetric changes, leading to enhanced bond strength.

7. Allowing sufficiently long setting times, such as mitigating the rapid setting of Sealant S4, during initial temperature increase proved advantageous. This could potentially be applied to other sealants to enhance their bonding performance with metal casing.
8. Accelerated corrosion not only induced corrosion at the sealant/casing interface but also affected the curing process, contributing to the observed bond enhancement. The low-frequency impedance response, particularly the capacitive component, could serve as a useful indicator for detecting corrosion initiation at the sealant/casing interface.
9. Comparisons between shear-bond and electrical testing revealed an unexpected correlation between bulk resistance and compressive strength. No correlation was found between bulk resistance and mean bond strength, as one would expect. Conductance measurements exhibited trends associated with sealant permeability. With appropriate consideration of influencing factors such as pore solution conductivity, electrical measurements have the potential to provide additional insights into sealant permeability.

Acknowledgement:

The CEMENTTEGRITY project is funded through the ACT programme (Accelerating CCS Technologies, Horizon2020 Project No 691712). Financial contributions from the Research Council of Norway (RCN), the Netherlands Enterprise Agency (RVO), the Department for Energy Security and Net Zero (DESNZ, UK), and Wintershall DEA are gratefully acknowledged.



References:

Adobe Photoshop. Photomerge. Available at www.adobe.com/uk/products/photoshop.html

Mabeyo PE, Ibrahim YS, Gu J, 2020. Effect of high metakaolin content on compressive and shear-bond strengths of oil well cement at 80°C. *Construction and Building Materials*, 240, 117962. <https://doi.org/10.1016/j.conbuildmat.2019.117962>

Kamali M, Khalifeh M, Eid E, Saasen A, 2022. Experimental study of hydraulic sealability and shear bond strength of cementitious barrier materials. *Journal of Energy Resources Technology*, 144(2), JERT-21-1253, 023007. <https://doi.org/10.1115/1.4051269>